

POLITECNICO DI TORINO

Commission of Mechanical, Aerospace, Automotive and

Production Engineering

Master's Degree in Automotive Engineering



Master's Degree Thesis

**Hybrid car regenerative braking system reverse  
engineering and modelling from track testing analysis**

Academic advisor:

Prof. Paolo Stefano Crovetti

Company advisor:

Ing. Patrick Gioffrè

Grazia Ponzano

Academic Year 2021-2022



## ABSTRACT

Hybrid powertrains for vehicles have been widely developed in recent years and spread in the market with the double goal of reducing fuel consumption and improve performance.

The integration of traditional internal combustion engine and electrical system can occur according to different layouts and control logics and may affect vehicle dynamics.

In this thesis work a parallel hybrid supercar has been analysed, investigating how its powertrains cooperate. The vehicle layout and a description of all the different ways in which the electric system and international combustion engine can be combined, can be found in the following chapters.

The employment of a hybrid layout enables the possibility to recover energy while travelling thanks to the use of the electric motors as generators, thus increasing the energy available and enhancing the electric driving range of the vehicle.

The study of the energy recovery active system has been the main focus of the thesis activity and is described in this report. Through a process of reverse engineering the logics behind the regenerative braking system have been explored starting from the analysis of the signals collected during track testing activities.

For a better understanding of how tests have been performed, in the first part of this report the common layout of sensor positioning and the standard manoeuvres performed are described, with an eye on the electrical acquisition and elaboration.

Focus of this thesis work has been the study of the electric traction's components behaviour during braking manoeuvres, in order to identify their role in the energy recovery process and understand logics and limits occurring.

Through the analysis of the dynamic response of the vehicle to the imposed input, a simplified model of the vehicle braking system has been developed and validated thanks to a process of co-simulation with a model of the whole vehicle already existing.

Final part of this paper is dedicated to the comparison of the signals obtained through the simulation process with those collected during the track tests sessions. This process gave satisfactory results confirming the accuracy of the analysis and of the developed simulation model.

## INDEX

ABSTRACT.....	I
LIST OF SYMBOLS .....	IV
INTRODUCTION .....	V
SOMMARIO .....	VIII
1. VEHICLE DYNAMIC BACKGROUND.....	1
1.1. TYRE BEHAVIOUR.....	1
1.1.1. LONGITUDINAL BEHAVIOUR.....	2
1.1.2. LATERAL BEHAVIOUR.....	5
1.1.3. LONGITUDINAL AND LATERAL FORCES INTERACTION.....	9
1.2. VEHICLE LATERAL DYNAMICS .....	11
1.3. STANDARD MANOEUVRES FOR HANDLING .....	15
1.3.1. STEADY STATE MANOEUVRES.....	15
1.3.2. TRANSIENT MANOEUVRES.....	17
1.4. VEHICLE LONGITUDINAL DYNAMICS .....	20
1.5. STANDARD MANOEUVRES FOR LONGITUDINAL DYNAMICS	22
2. VEHICLE SENSORS SETUP FOR TESTING .....	23
2.1. SENSORS .....	23
2.1.1. ACCELEROMETERS .....	24
2.1.2. INERTIAL MEASUREMENT UNIT .....	25
2.1.3. OPTICAL SENSORS .....	27
2.1.4. LOAD CELLS .....	29
2.1.5. STEERING ANGLE, TORQUE AND SPEED SENSORS .....	30
2.1.6. LINEAR POSITION SENSOR.....	31
2.2. GLOBAL LAYOUT .....	33
2.3. DATA COLLECTION.....	36

---

3.	REGENERATIVE BRAKING REVERSE ENGINEERING.....	38
3.1.	CASE STUDY: PLUG-IN HYBRID VEHICLE LAYOUT .....	38
3.2.	DRIVE MODES.....	41
3.3.	REGENERATIVE BRAKING: THEORETICAL BACKGROUND ...	44
3.3.1	ELECTRONIC BACKGROUND FOR ELECTRIC MOTORS .....	46
3.3.2	BRUSHLESS MOTORS .....	49
3.3.3	BLDC MOTORS COMMUTATION.....	51
4.	DATA ANALYSIS .....	57
4.1.	BRAKE STEP MANOEUVRE .....	57
4.2.	DECELERATION PROFILE EVALUATION .....	60
4.3.	ELECTRIC MOTORS SIGNALS .....	62
5.	VEHICLE MODEL .....	67
5.1.	MODEL DEVELOPMENT .....	67
5.1.1.	TOTAL BRAKING TORQUE REQUIRED .....	69
5.1.2.	MAXIMUM CHARGING POWER ADMISSIBLE BY THE BATTERY .....	71
5.1.3.	ACTUAL POWER REGENERABLE BY ELECTRIC MOTORS .....	72
5.1.4.	BRAKING TORQUE SPLIT BETWEEN ELECTRICAL AND MECHANICAL.....	76
5.1.5.	VARIATION OF BATTERY STATE OF CHARGE .....	77
5.2.	MODEL VALIDATION.....	78
5.2.1.	CO-SIMULATION DESIGN .....	79
5.2.2.	RESULTS ANALYSIS.....	81
	CONCLUSIONS AND FUTURE DEVELOPMENT.....	88
	BIBLIOGRAPHY.....	90
	LIST OF FIGURES .....	91
	ACKNOWLEDGEMENTS.....	94
	RINGRAZIAMENTI.....	95

## LIST OF SYMBOLS

$\alpha$	wheel side slip angle
$\beta$	vehicle side slip angle
$\gamma$	wheel camber angle
$\omega$	rotational speed
R	wheel radius
$\sigma$	longitudinal slip
$\mu$	friction coefficient
$\psi$	yaw angle
$\dot{\psi}$	yaw rate
$\delta$	steering angle
l	wheelbase
a	front axle distance from centre of gravity
b	rear axle distance from centre of gravity
$C_x$	drag coefficient
$C_z$	lift coefficient
$\rho$	air density
$\alpha$	road inclination angle
T	torque
P	power
fem, $\varepsilon$	back electromotive force
i	current
V	voltage
D	duty cycle

## INTRODUCTION

The present master thesis has been developed in collaboration with Danisi Engineering s.r.l. within February and September 2022 as final work for the Automotive engineering degree.

This report focuses on the analysis of a hybrid vehicle signals and data collected during track tests and on understanding the logics behind its regenerative braking system through a reverse engineering process.

The analysed vehicle is a parallel hybrid supercar, composed of a traditional internal combustion engine on the rear axle and three electric motors: one of them close-coupled with the engine in P1 position and the other two on the front axle in P4 position.

By combining these electric motors with the internal combustion engine unit, the all-wheel drive traction can be activated. The presence of the two front electric motors enables the energy recuperation and transfer to the battery during braking events, such to increase the battery state of charge and enhance the electric drive range.

In order to analyse the control logics behind the regenerative braking system, track test sessions have been performed and signals coming from sensors and from vehicle network have been collected.

Road testing activities have been focused on standard manoeuvres defined by the company to test vehicle handling and braking performance. The latter ones have been tested through Brake-step manoeuvres, performed braking at constant pedal stroke and on straight road.

To give a complete comprehension of the recorded signals, the first chapters of this thesis focus on a description of how the manoeuvres have been performed. Moreover, the procedure to prepare the vehicle for track testing is described, with a detailed focus on each employed sensor's characteristics.

At first, the collected data have been analysed through the acquisition system's software, then exported in *Matlab* environment for the post-process.

By analysing the signals recorded from electric traction components, it has been evident that some unexpected behaviour of parameters such as electrical braking torque was present and the reasons behind have been investigated.

The main part of this thesis work, indeed, focuses on the study and research of variables that may affect the energy recuperation during braking manoeuvres, both bibliographically and experimentally, by analysing each component involved in the event itself.

Electric motors, high voltage battery and inverter characteristics have been analysed in detail, with main focus on the latter one's control logics as ended up being of primary importance.

The inverter's behaviour, indeed, is strongly influenced by electrical motors' rotational speed as when it varies, also back electromotive force does. The energy transfer from e-motors to battery is controlled by the inverter itself by managing both current and voltage at stator's windings level.

When the rotational speed falls below a certain threshold, anyway, the inverter is no longer able to manage those parameters such to let them be coherent to battery recharge needs, so the energy transfer is interrupted and regeneration ends, with a decrease in electric braking torque.

In order to maintain the desired deceleration profile, evaluated through manoeuvre analysis as function of initial speed, brake demand and battery state of charge, the hydraulic brake intervention is needed. A study of this brake torque split is performed in this thesis.

The final part of this report, once evaluated the brake control unit and electric traction components' control logics, is dedicated to the description of how a simulation model in *Simulink* environment has been developed.

The model aims to replicate the vehicle behaviour during straight braking events, to be compared with the one recorded during track tests and involves a study on the battery parameters too to analyse the variation of the state of charge and the power flows.

The brake model validation has been performed with a co-simulation process through which the integration of the model itself with a complete vehicle model was possible.

The co-simulation enabled the possibility of replicating the manoeuvres performed on the test track in a realistic way, taking in consideration important variables not analysed in the single brake model only, such as load distribution or tires and suspensions characteristics.

The simulated manoeuvres have been compared to those recorded during tests sessions, ending up having coherent results both from vehicle dynamics point of view with the deceleration profile analysis and from the electronic parameters point of view, with electric motors braking torque and power flow analysis.

The coherence between recorded and simulated signals confirms the correctness of the work.

The developed model and all the analysis are reported in this thesis.

## SOMMARIO

Il presente elaborato riporta il lavoro di tesi svolto in collaborazione con l'azienda Danisi Engineering s.r.l. nei mesi tra febbraio e settembre 2022, volto alla preparazione dell'esame finale di laurea magistrale in Ingegneria dell'Autoveicolo.

Il lavoro si concentra sull'analisi dei dati e dei segnali di un veicolo ibrido raccolti durante test su strada per ricavare mediante un processo di reverse engineering le logiche di controllo del sistema di frenata rigenerativa.

L'automobile in esame è un veicolo sportivo ibrido parallelo, composto da un motore termico posteriore e da tre motori elettrici: uno di essi posizionato sull'assale posteriore in configurazione P1 mentre gli altri due posizionati sull'assale anteriore, in configurazione P4.

L'utilizzo dei motori elettrici anteriori combinato con il motore termico posteriore garantisce al veicolo la possibilità di azionare la trazione integrale. La presenza dei motori elettrici anteriori, inoltre, permette il recupero di energia durante la frenata ed il trasferimento verso la batteria, con il fine di incrementare lo stato di carica della batteria e di aumentare pertanto l'autonomia di guida elettrica.

Con l'obiettivo di analizzare le logiche di controllo di questo sistema di frenata rigenerativa, sono state svolte sessioni di test in pista ed i segnali di diversi sensori e della rete veicolare sono stati raccolti con un sistema di acquisizione predisposto.

In particolare, le prove su strada si sono concentrate sulle manovre standard definite dall'azienda per il controllo della manovrabilità dell'auto e su manovre di frenata su rettilineo a pressione sul pedale del freno costante, definite manovre brake-step.

I primi capitoli di questo elaborato si concentrano pertanto sul richiamo dei concetti teorici importanti per l'analisi dinamica del veicolo, con la descrizione dettagliata di come vengono svolte le manovre di test.

Inoltre, la metodologia di equipaggiamento del veicolo durante la preparazione per le prove su strada viene descritta con una attenta analisi di ogni sensore comunemente impiegato e del suo collegamento con il sistema di acquisizione.

I dati collezionati sono stati analizzati dapprima attraverso il software di raccolta dei segnali, dopodiché esportati in ambiente *Matlab* per l'elaborazione.

La verifica dei segnali raccolti dai motori elettrici e dal sistema di trazione elettrica globalmente hanno individuato comportamenti inattesi e ripetibili degli stessi, come l'andamento non crescente della coppia frenante generata dai motori elettrici e di conseguenza la non costanza nella potenza recuperata.

La fase centrale del lavoro si è quindi incentrata sulla ricerca di variabili che potessero influenzare il recupero dell'energia in frenata analizzando, sia a livello bibliografico che sperimentalmente, ogni componente interessato dall'evento.

In particolare, le caratteristiche dei motori, della batteria e dell'inverter sono state analizzate, con maggior attenzione sulle logiche di controllo dell'inverter che si sono rivelate determinanti. Il comportamento di quest'ultimo, infatti, viene molto influenzato dalla velocità rotazionale dei motori elettrici, poiché al variare della stessa varia la forza elettromotrice indotta.

Il trasferimento dell'energia dai motori elettrici alla batteria viene gestito dall'inverter che gestisce i livelli di tensione e corrente uscente dagli avvolgimenti degli statori.

Al di sotto di una velocità rotazionale minima, tuttavia, questo meccanismo non può essere attuato e la rigenerazione viene interrotta, con conseguente diminuzione della coppia elettrica frenante.

Particolare attenzione è stata rivolta all'intervento dei freni idraulici per compensare la coppia totale frenante richiesta dal pilota, con il fine di mantenere coerente il profilo di decelerazione atteso, ricavato attraverso l'analisi di numerose manovre e funzione di velocità iniziale, corsa pedale del freno e stato di carica della batteria.

Ricavate le logiche di controllo della centralina frenante e dei componenti coinvolti nella rigenerazione, il lavoro di tesi si è concentrato sullo sviluppo di un modello virtuale in ambiente *Simulink* per replicare il comportamento del veicolo durante le manovre di frenata svolte in pista. Il modello sviluppato comprende anche lo studio delle di gestione dalla batteria, analizzando l'incremento di carica e il livello di potenza entrante.

La validazione del modello è stata svolta attraverso un processo di cosimulazione che ha permesso di integrare il modello del veicolo completo preesistente con il modello sviluppato della centralina freni.

In questo modo le manovre replicate e l'analisi dei dati sono stati realistici e completi di variabili del veicolo precedentemente non considerate, come la distribuzione esatta dei carichi, le caratteristiche degli pneumatici e del sistema sospensivo.

I test replicati virtualmente hanno riportato un andamento coerente con quanto precedentemente registrato in fase di manovre in pista, sia a livello di dinamica del veicolo con l'analisi del profilo di decelerazione, sia a livello elettronico con l'analisi delle coppie frenanti generate dai motori elettrici e dei flussi di potenza trasferiti in batteria.

La coerenza del modello virtuale con il comportamento reale del veicolo ha confermato la correttezza del lavoro svolto.

Il modello studiato e le analisi comparative dei test sono riportati nell'elaborato.

---

*This page is intentionally left blank*

## 1. VEHICLE DYNAMIC BACKGROUND

Vehicle dynamics can be defined as “the study of how the vehicle will react to external inputs”, that could be external forces, driver commands or ambient conditions.

Having a good control on the vehicle dynamics is important in order to reach better vehicle control, higher safety and higher customer satisfaction.

Vehicle dynamics is affected by the characteristics of the vehicle such as weight distribution, drivetrain, tyres and braking type, steering and suspensions geometries, or by external environment, as aerodynamics. As vehicles are mechanical systems, described by nonlinear equations, they can be studied by a mathematical model. The choice of the right model depends on the application and on the level of approximation desired.

In this chapter an overview on the basics of vehicle dynamics is given, introducing the main activity of reverse engineering.

### 1.1. TYRE BEHAVIOUR

Since the contact between the vehicle and the ground occurs via the tyres, made by deformable material, it is worth to recall basic concepts about how tyre forces are generated and transferred to ground during traction or braking conditions.

The analysis of this paragraph will be based on the reference system in Figure 1, with the origin in the contact point between tyre and ground, X axis forward, Z axis upward and perpendicular to ground, Y axis directed accordingly.  $\alpha$  is the wheel Side slip angle while  $\gamma$  the Camber angle<sup>[2]</sup>.

Considering a portion of the tyre contact patch, the pressure will be distributed on a relatively wide surface and not limited on a single point: this will give rise to resultant forces both in lateral and in longitudinal direction. These forces distribution will be affected by many operating parameters as tyre structure, pressure, load, or road conditions. Moreover, when changing the vertical load, the normal force changes subjected to hysteresis; this effect of vertical force damping is much more present at low speed than at high speed.

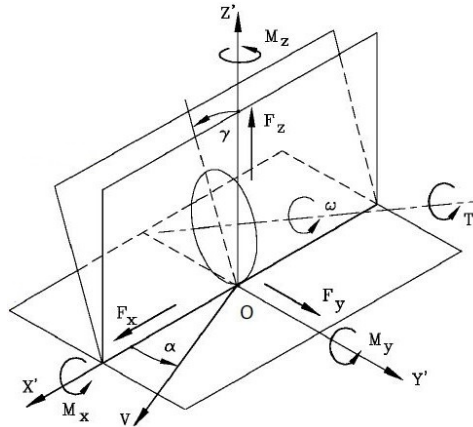


Figure 1: Wheel reference frame

### 1.1.1. LONGITUDINAL BEHAVIOUR

Considering an undeformable wheel rolling on an undeformable surface, the relationship between angular and longitudinal speed would be given by the equation  $V = \omega_0 \cdot R_0$ , where  $R_0$  is the radius of the wheel.

Since vehicle wheels are covered by deformable tyres, the latter relation does not hold anymore, and the radius  $R$  must be replaced by an effective radius  $R_e$ , considering the instantaneous point of rotation instead of the contact point on the ground.

Considering a wheel subjected to braking moment, the distribution of normal and tangential forces will be the one depicted in the Figure 2a:

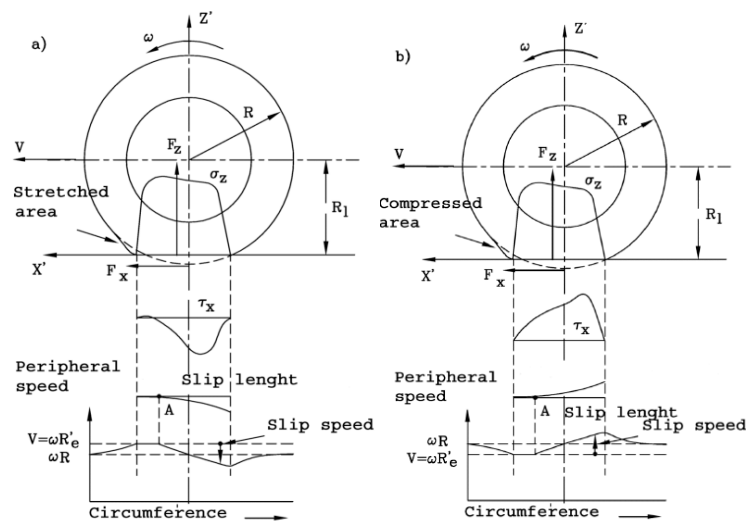


Figure 2: Contact pressure distribution during braking and traction

The part of the tyre in contact with the ground will be subjected to traction condition, instead of being compressed as in pure rolling. Contact patch local velocity will rise, being higher than the undeformable wheel's one  $\omega_0 \cdot R_0$ . This will result in  $R_e > R_0$ , being  $R_e$  the effective radius in braking condition, shifted toward ground (point C' in Figure 3).

On the contrary, during traction phase (Figure 2b), the contact patch will be compressed instead of being tractioned as in pure rolling, ending up having a larger angular wheel velocity with respect to the pure rolling  $\omega_0$ . Instant centre of rotation will be shifted upward with respect to ground,  $R_e < R_0$  (point C'' in Figure 3).

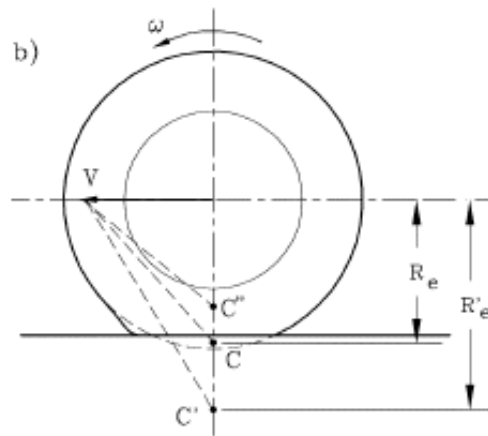


Figure 3: instant point of rotation in pure rolling C, braking C' and traction C''

It is then possible to define a parameter to define how much the angular wheel speed differ from the pure rolling one, called *Longitudinal Slip*  $\sigma$ :

$$\sigma = \frac{\omega - \omega_0}{\omega_0} = \frac{R_0 - R}{R}$$

It can be defined as the formula above or in percentage. Longitudinal slip is positive in traction condition while negative in braking. Moreover, two limit cases can be identified:

- Blocked wheel:  $\omega=0$ ,  $\sigma = -1$
- Slipping wheel:  $V=0$ ,  $\sigma = +\infty$ .

The longitudinal force  $F_x$  transmissible to ground is function of Slip. When the latter increases numerically from zero, the force rises rapidly and linearly to a maximum, which usually occurs for a value of slip in the range of 0.1-0.15, then tend to decrease. This

behaviour is shown in Figure 4. To obtain the maximum longitudinal force to drive the vehicle, a deformation of the tyre contact patch and a non-null slip is needed.

It is reasonable to assume that longitudinal force at constant  $\sigma$  is proportional to the vertical force  $F_z$ , so a Friction Coefficient  $\mu_x$  can be defined as:

$$\mu_x = \frac{F_x}{F_z}$$

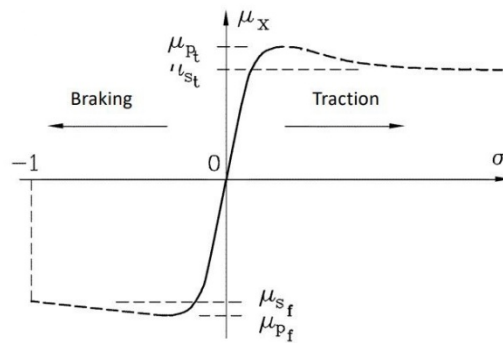


Figure 4: Longitudinal friction coefficient as function of slip

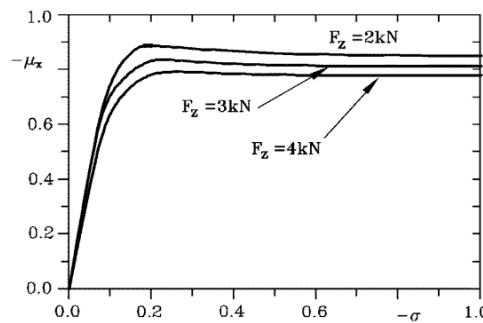


Figure 5: Longitudinal friction coefficient as function of slip and  $F_z$

In Figure 5 is possible to see how in reality the longitudinal force is not truly proportional to vertical force: when increasing the vertical force, the longitudinal one has a lower peak occurring at higher slip values.

This trend can be synthesized in saying that lower vertical forces correspond to larger friction coefficient and so that lighter vehicles are capable to develop larger accelerations for the same tyre set.

Friction coefficient is affected by road conditions, speed and water layer on the ground. The relation between the vertical load and the longitudinal force as function of slip can be described by the empirical equation proposed by H.B. Pacejka, known as the *Magic Formula*:

$$F_x = D \cdot \sin(C \cdot \arctan\{B(1 - E)(\sigma + S_h) + E \cdot \arctan[B(\sigma + S_h)]\}) + S_v$$

Where the coefficients are obtained as data fitting of experimental tyre data.

### 1.1.2. LATERAL BEHAVIOUR

As for longitudinal dynamics the forces from tyres can be transmitted to the ground only for non-null values of slippage, the same concept can be retrieved for lateral forces too. When a vehicle is cornering at non negligible speed a Side slip angle  $\alpha$  is generated, the shape of the contact patch of the tyre is distorted and the wheel velocity do not lie in its midplane.

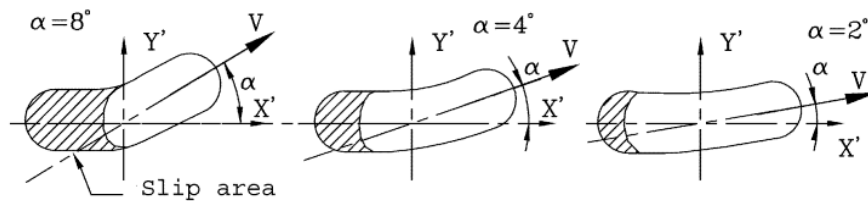


Figure 6:Distorsion of contact patch

Thanks to the presence of a side slip angle, the vehicle is needed to generate side forces and corner. For sign convention, it is needed to underline that positive side slip angle generates a negative lateral force.

In Figure 7 pressure and slip distribution of a cornering wheel is reported. It is possible to notice how the resultant lateral force  $F_y$  is not lying on the centre of the contact patch but moved rearward of a distance  $t$ . This will result in the generation of a *Self-aligning Torque*  $M_z$ , that tends to realign the wheel axis to the direction of speed, reducing  $\alpha$ .

$$M_z = F_y \cdot t$$

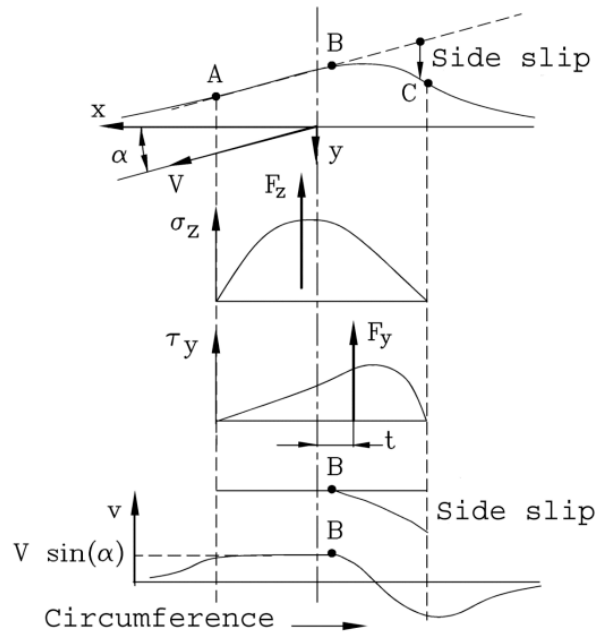


Figure 7: Pressure and slip distribution of a cornering tyre

Increasing the side slip angle  $\alpha$ , the lateral force  $F_y$  increase linearly in the first part then remains almost constant. The pressure distribution instead become more uniform when increasing  $\alpha$ , leading to a decrease of the distance  $t$  between the resultant force and the wheel centre. As a result, the self-aligning torque  $M_z$  has a distribution as the one reported in Figure 8:

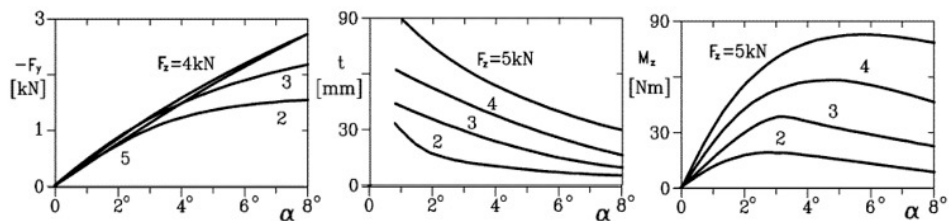


Figure 8: Lateral force, caster trail and self-aligning torque as function of slip angle

For high values of side slip angle, the self-aligning torque may also become negative and increase the angle  $\alpha$  even more.

It is also possible to define a coefficient linking the lateral force  $F_y$  to the side slip angle  $\alpha$ , known as the *Cornering Stiffness C*, and represented by the secant of the  $F_y - \alpha$  plot.

$$C = -\frac{F_y}{\alpha}$$

For a given load, the cornering stiffness decreases when increasing  $\alpha$ , while it increases linearly with the vertical load until a value above which it remains constant. Due to this behaviour, cornering stiffness can be approximated by the following bilinear graph:

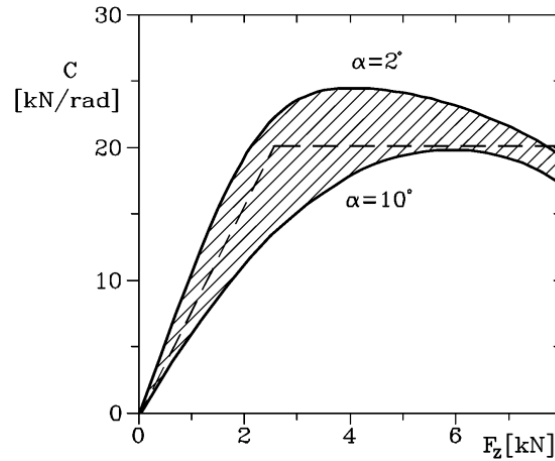


Figure 9: Cornering stiffness as function of vertical load

The lateral force is usually replaced by the Side friction coefficient  $\mu_y$ , that allows to normalize the side force with respect to the vertical one.

$$\mu_y = \frac{F_y}{F_z}$$

Both side force and self-aligning torque are affected by many factors as pressure, normal force or road conditions. The global lateral behaviour of the tyre can be synthesised by the Gough diagram in which the side force  $F_y$  is expressed as function of  $M_z$ , with  $\alpha$  and  $t$  as parameters.

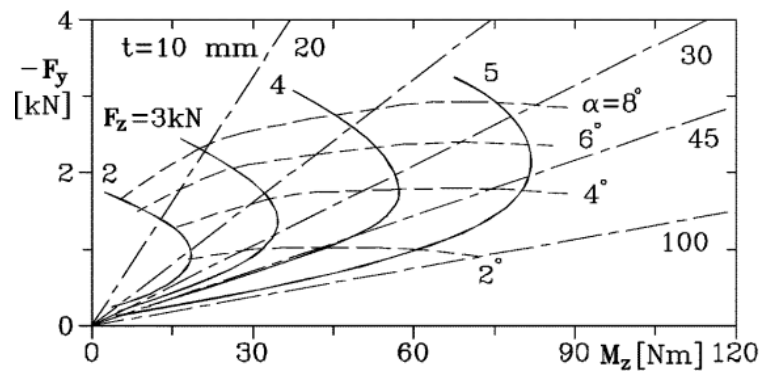


Figure 10: Gough diagram

It is worth to notice that there is no correspondence between peak of lateral force and of self-aligning torque one, which occurs much earlier. It is also possible to notice that the peak of lateral force that can be transmitted to ground falls off as the load increase: this effect is called *tyre load sensitivity*.

Lateral force is also generated by the presence of a non-zero *Camber angle*  $\gamma$ , defined as the angle between the tilted wheel plane and the vertical one, as depicted in Figure 1. This lateral force is usually called *Camber force*, to distinguish from the *Cornering force*, the one produced by sideslip angle  $\alpha$ . The sum of the two gives the total side force, able to balance the side component of the vertical force.

$$F_y = F_{y,\alpha} + F_{y,\gamma} = F_z \cdot \tan\gamma$$

Usually, the camber angle contribution to the side force is lower than the side slip angle one, at least for equal values of  $\alpha$  and  $\gamma$  and is highly dependent on vertical load and type of tyre.

The camber force is not applied on the centre of contact patch, but ahead it of a small quantity that will give rise to a small moment  $M_{z,\gamma}$  usually neglected.

Self-aligning torque increase proportionally with camber angle.

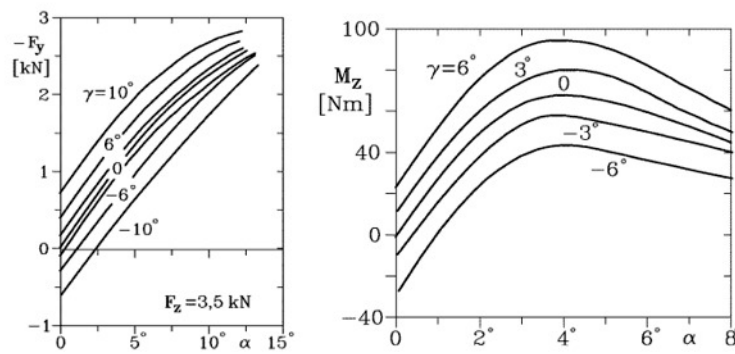


Figure 11: Effect of camber angle on Side force and Self-aligning torque

The relation between the vertical load and the longitudinal force as function of slip can be described by the empirical equation proposed by H.B. Pacejka, known as the *Magic Formula*:

$$F_y = D \cdot \sin(C \cdot \arctan\{B(1 - E)(\alpha + S_h) + E \cdot \arctan[B(\alpha + S_h)]\}) + S_v$$

Where the coefficients are obtained as data fitting of experimental tyre data.

## 1.1.3. LONGITUDINAL AND LATERAL FORCES INTERACTION

When longitudinal and lateral tyre characteristics are combined, as when driving or braking while cornering, the behaviour described above change considerably. The adherence gain in one of the two direction, in fact, reduces the adherence on the other one.

The same will occur for lateral and longitudinal forces: it won't be possible to obtain the maximum of one force if also the other one must be generated.

Comparing longitudinal and lateral friction coefficient as function of slip in Figure 12, it can be seen that they follow different trends: the lateral one peaks for null slip, while the longitudinal one peaks for values of slip in the range 0.1-0.15. It is reasonable to conclude that to be able to both generate high lateral force and high longitudinal one, slip must be kept low.

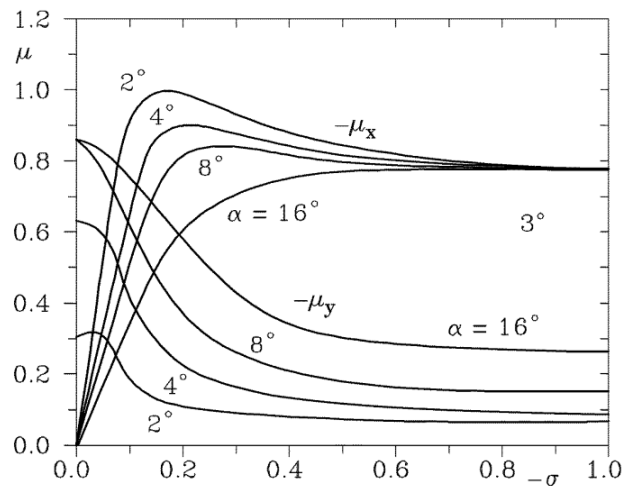


Figure 12: Interaction between longitudinal and lateral slip

The combined effect of longitudinal and lateral forces generated on the tyres can be synthesised in the diagram below, which contains lateral friction coefficient as function of longitudinal one, including the effect of slip and side slip angle. The graph on the left is diagrammed as function of the forces  $F_y - F_x$ , while the one on the right as function of friction coefficients  $\mu_y - \mu_x$ .

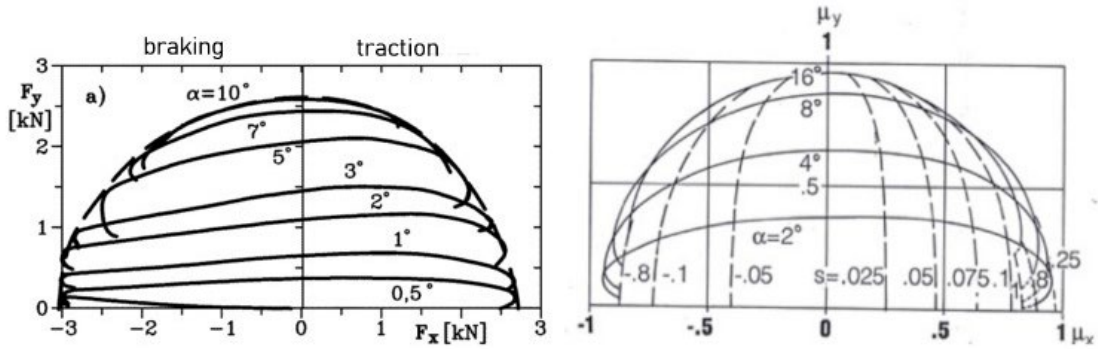


Figure 13: Polar diagram of force exerted on tyres. a) experimental b) elliptical approximation

From experimental data it is possible to notice how the lateral force decreases when increasing the longitudinal slip  $\sigma$  both in traction and in braking, and how the maximum longitudinal force decreases with increasing side slip angle  $\alpha$  both in traction and in braking.

The experimental data are usually replaced by an elliptical approximation, expressed by the formula

$$\left(\frac{F_x}{F_{x0}}\right)^2 + \left(\frac{F_y}{F_{y0}}\right)^2 = 1$$

Where  $F_{x0}$  and  $F_{y0}$  are, respectively, the maximum longitudinal force exerted at zero sideslip angle and the force  $F_y$  exerted at the given sideslip angle when no force  $F_x$  is exerted.

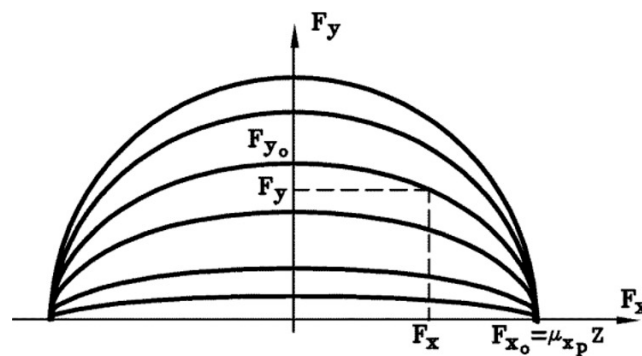


Figure 14: Elliptical model approximation

The model is currently used in any automotive application with the strong assumption to have the same maximum longitudinal force regardless of the value of the sideslip angle  $\alpha$ .

## 1.2. VEHICLE LATERAL DYNAMICS

The relevant variables when analysing lateral vehicle dynamics are mainly three: vehicle side slip angle  $\beta$ , yaw angle  $\psi$  and yaw angular velocity  $\dot{\psi}$  (or  $r$ ).

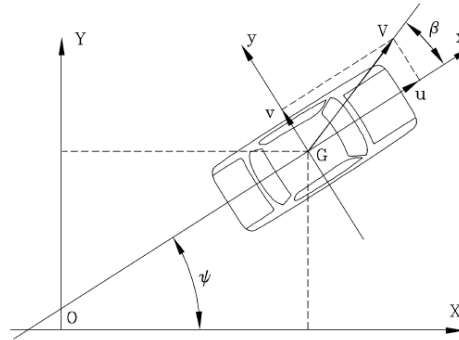


Figure 15: Vehicle fixed and local reference frame

Assuming the fixed reference frame  $X, Y, Z$  and the local reference frame  $x, y, z$  centred in the vehicle center of gravity depicted in the scheme below, with  $Z$  and  $z$  oriented according to the right hand rule, it is possible to define the Side slip angle  $\beta$  as the angle between the longitudinal axis of the vehicle and the velocity vector. The Yaw angle  $\psi$  instead can be defined as the angle between the longitudinal axis of the vehicle and the  $X$  axis of the fixed reference frame. The Yaw angular velocity or Yaw rate  $\dot{\psi}$  is the angular velocity of the vehicle around the vertical axis  $Z$ .

The simplest model that can be used for lateral dynamics is the so-called *bicycle model*, represented below:

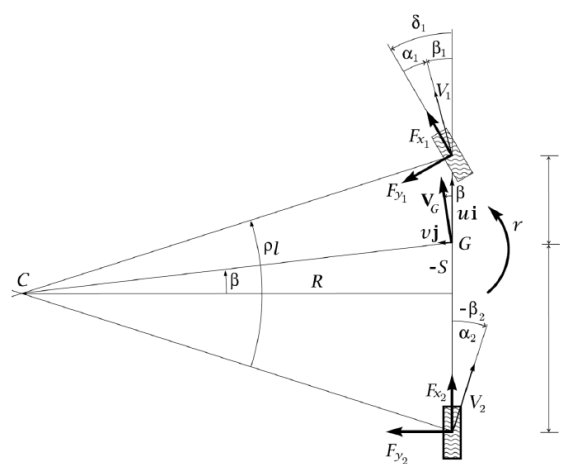


Figure 16: Bicycle model reference frame

This model can be considered as well representing vehicle dynamics in *kinematic steering* conditions, with these main assumptions:

- The vehicle is a rigid body
- The speed is low so to neglect aerodynamic forces contribution
- The motion is on flat and horizontal surface
- Radius of curvature is much higher than wheelbase  $R \gg l$ , so  $\alpha_i, \delta_i$  are small angles.

Under these conditions, lateral acceleration can be neglected due to low and constant speed, so no lateral forces on the wheels will arise and consequently, vehicle will be in pure rolling conditions.

Steering wheel angle and side slip angle can be evaluated by geometrical considerations:

$$\begin{aligned} R &= l \cdot \cot g(\delta) \approx \frac{l}{\delta} & \delta_{kin} &= \frac{l}{R} \\ R &= b \cdot \cot g(\beta) \approx \frac{b}{\beta} & \beta_{kin} &= \frac{b}{R} \end{aligned}$$

As soon as vehicle speed increase and lateral acceleration can no longer be neglected, wheels will have slip angles  $\alpha$  different from zero and generate lateral forces: this condition is no longer of kinematic steering but must be considered *dynamic steering*.

Considering the equilibrium on the y axis (perpendicular to vehicle longitudinal axis), and around z axis, it is possible to obtain the expression of the side forces:

$$F_{x1} \sin(\delta_1) + F_{y1} \cos(\delta_1) + F_{y2} = \frac{mV^2}{R} \cos(\beta)$$

From the hypothesis of angles to be small;

$$\begin{aligned} F_{y1} + F_{y2} &= \frac{mV^2}{R} \\ F_{y1} \cdot a &= F_{y2} \cdot b \end{aligned}$$

Solving these two equations front and rear side forces are obtained

$$\begin{aligned} F_{y1} &= \frac{mV^2 b}{R l} \\ F_{y2} &= \frac{mV^2 a}{R l} \end{aligned}$$

As well, side forces can also be expressed as:

$$F_{yi} = C_i * \alpha_i$$

Where  $C_i$  is the cornering stiffness of the axle  $i$ , assumed to be in the linear range, while  $\alpha_i$  is the slip angle, defined as the angle between the axis of the wheel and the direction of speed vector and given by the formula

$$\alpha_1 = \frac{mV^2}{R} \frac{b}{lC_1}$$

$$\alpha_2 = \frac{mV^2}{R} \frac{a}{lC_2}$$

An important parameter for lateral dynamics is the Side slip angle  $\beta$ , representing the angle between the longitudinal axis of the vehicle and the direction of motion.

It is useful to characterize the cornering behaviour of the vehicle, i.e. its under or oversteering attitude. It can be evaluated from geometrical construction, together with the steering angle  $\delta$ .

$$\beta = \arctan \frac{b}{R} - \tan \alpha_2 \cong \frac{b}{R} - \alpha_2 = \beta_{kin} - \alpha_2$$

$$\tan(\delta - \alpha_1) = \frac{a}{R} + \beta = \frac{a}{R} + \frac{b}{R} - \alpha_2$$

$$\delta \cong \frac{l}{R} + \alpha_1 - \alpha_2 = \delta_{kin} + \alpha_1 - \alpha_2$$

A good indicator of the vehicle lateral dynamics is the so-called curvature gain: the rate of change of curvature  $\rho$  when changing the steering angle

$$\rho = \frac{1}{R}$$

$$\frac{1}{R\delta_1} = \frac{1}{l} \cdot \frac{1}{1 + \frac{mV^2}{l^2} \left( \frac{bC_2 - aC_1}{C_1C_2} \right)} = \frac{1}{l} \cdot \frac{1}{1 + KV^2}$$

Considering that in kinematic condition  $\frac{1}{R\delta_1} = \frac{1}{l}$ , we can consider the second term of the equation as a corrective factor to take into account the dynamics conditions of the vehicle. It is called *Understeer gradient* or Stability factor [rad/m/s<sup>2</sup>]:

$$K = \frac{m}{l^2} \left( \frac{bC_2 - aC_1}{C_1C_2} \right)$$

This parameter allows to describe the cornering tendency of the vehicle

- $K > 0$   $bC_2 > aC_1 \rightarrow$  Understeering behaviour
- $K < 0$   $bC_2 < aC_1 \rightarrow$  Oversteering behaviour
- $K = 0$   $bC_2 = aC_1 \rightarrow$  Neutral-steering behaviour

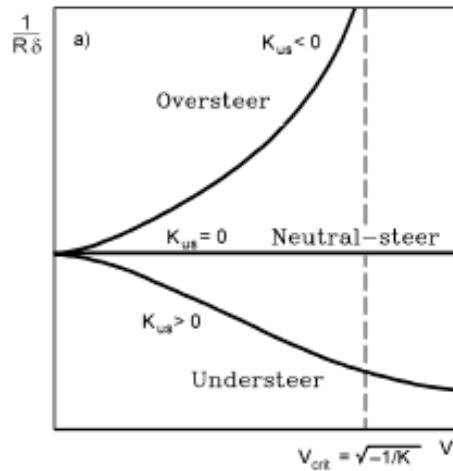


Figure 17: Understeering behaviour

Understeering and oversteering vehicles are characterized by having a Neutral point (point in which if any force is applied no yaw motion is produced) different from the centre of gravity: in the first case will be moved rearward, while in the latter forward. For further details refer to [2].

The following graph is also useful in recalling vehicle tendency to increase the curvature radius in understeering vehicle when accelerating or to reduce it in oversteering ones.

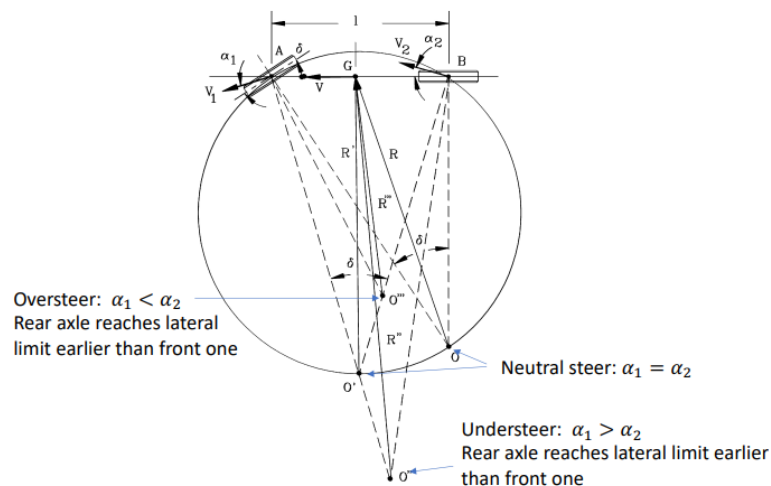


Figure 18: Understeering curvature radius behaviour

### 1.3. STANDARD MANOEUVRES FOR HANDLING

To test vehicle dynamics and handling, some standard manoeuvres are usually performed, according to what explicated by the norm ISO 15037-1. These tests allow to characterize the vehicle lateral steering behaviour, discriminating between understeering or oversteering ones, and comparing the trend of the main parameters with the kinematic ideal ones. Manoeuvres can be divided into steady state or transient ones.

#### 1.3.1. STEADY STATE MANOEUVRES

The most important manoeuvres to evaluate steady state cornering behaviour of a vehicle is the so called *Ramp Steer* manoeuvre.

It has to be performed in a track, starting in a straight and then gradually increasing the steering wheel angle with a constant rate. The speed must be kept constant along the whole test.

The initial straight path is needed in order to have initial null steering wheel angle and side slip angle as reference. The following graphs are referring to ramp steer manoeuvre performed with the vehicle under test in this thesis, at a constant speed of 100 km/h and with a steering wheel angle increasing from  $0^\circ$  to  $60^\circ$  in 5 seconds.



Figure 19: Steering angle during Ramp steer manoeuvre

It can be seen that the steering wheel angle increases linearly, so steering angle rate is sufficiently constant to consider the manoeuvre to be correct. These conditions well represent the kinematic ones, remaining in the linear range of cornering stiffness of tyres, so results of this test have been analysed and handling parameters evaluated based on kinematic steering equations reported above.

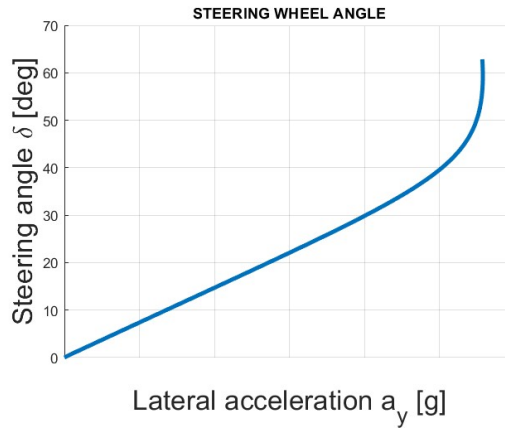


Figure 20: Steering angle as function of lateral acceleration during Ramp Steer manoeuvre

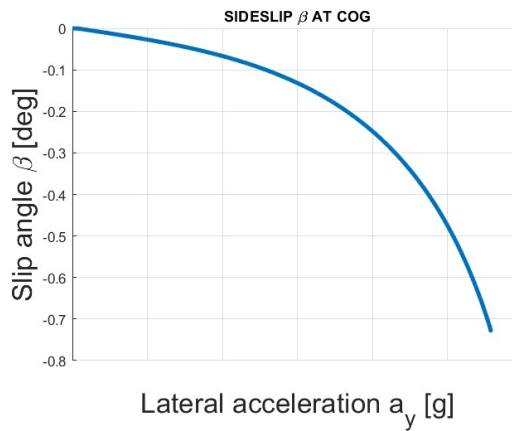


Figure 21: Side slip angle as function of lateral acceleration during Ramp Steer manoeuvre

From the equations above, substituting the formulation of the side slip angles on the wheels, it is possible to check how much the steering wheel angle in dynamic conditions differ from the kinematic one:

$$\delta = \delta_{kin} + \frac{mV^2}{R} \frac{b}{lC_1} - \frac{mV^2}{R} \frac{a}{lC_2}$$

$$\delta - \delta_{kin} = \left( \frac{m_1}{C_1} - \frac{m_2}{C_2} \right) \frac{V^2}{R} = K \frac{V^2}{R}$$

Where  $m_1$  and  $m_2$  are respectively the masses of the front and of the rear axle. The factor multiplying the lateral acceleration is the *Understeering gradient*  $K$ , described above.

From the plot of the steering wheel angle as function of the lateral acceleration it can be noticed that the vehicle behaves like neutral steering (linear increment of  $\delta$  with  $a_y$ ) until lateral acceleration reach high values. In that condition, the vehicle start to behave as understeering one.

The second graph can instead be analysed considering the *Side-slip gradient*  $K_\beta$ : it defines how the angle  $\beta$  changes according to the increment of lateral acceleration. It is a good indicator of handling performance of the vehicle cornering dynamics and can be evaluated starting from equation [rif] and from geometrical considerations. Side slip gradient shows how much the side slip angle differ from the kinematic one:

$$\beta = \beta_{kin} - \alpha_2 = \beta_{kin} - \frac{mV^2}{R} \frac{a}{lC_2}$$

$$\beta - \beta_{kin} = -\frac{m_2 V^2}{C_2 R} = -K_\beta \frac{V^2}{R}$$

Again, this parameter  $K$  shows the linear behaviour of the vehicle, close to kinematic one, for low lateral accelerations, while the behaviour deviates from kinematic conditions as soon as lateral acceleration increases.

It is important to remind that bicycle model well represents the cornering dynamics for low velocity and negligible lateral acceleration, up to 0.4g.

### 1.3.2. TRANSIENT MANOEUVRES

Transient manoeuvres are those intended to evaluate the dynamic stability of the vehicle, so the ability to retrieve its equilibrium condition after the end of a perturbation. A common test to understand this transient vehicle behaviour is the *Step Steer Manoeuvre*, according to ISO7401.

It consists in a test performed on a test rig at constant velocity. The driver must start the test with a straight line, in order to have initial null steering wheel angle and side slip, then move the steering wheel to a specific angle and keep it constant for a short time, usually of 3 seconds, after which leave the steering wheel and wait for the vehicle to come

back to equilibrium conditions. Usually, this test is performed at a steering angle rate of  $300^\circ/\text{s}$ .

The graphs below show an example of Step steer manoeuvre, performed at 100 km/h with an imposed steer angle of  $25^\circ$ , producing a lateral acceleration of around 0.6g.

Time history of yaw rate, side slip angle and steering angle are reported and are important to characterise vehicle transient dynamic.

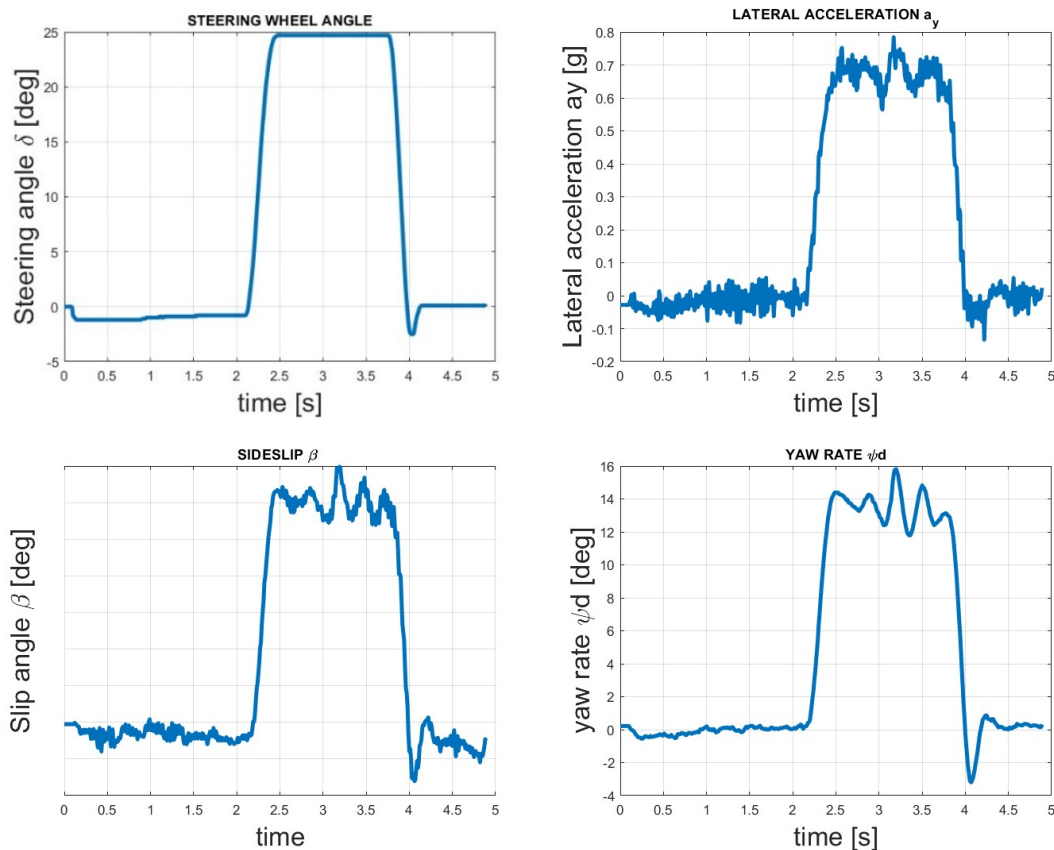


Figure 22: Steering angle, lateral acceleration, slip angle and yaw rate trend during step steer manoeuvre

They allow to evaluate the amount of delay present between the input from the driver and the response of the system, in particular analysing the one between the constant phase of steering angle and the one of yaw rate. Response time are defined with respect to a line crossing 10% and 90% points of steering angle input, where the line crosses the zero steering angle the zero time is assumed.

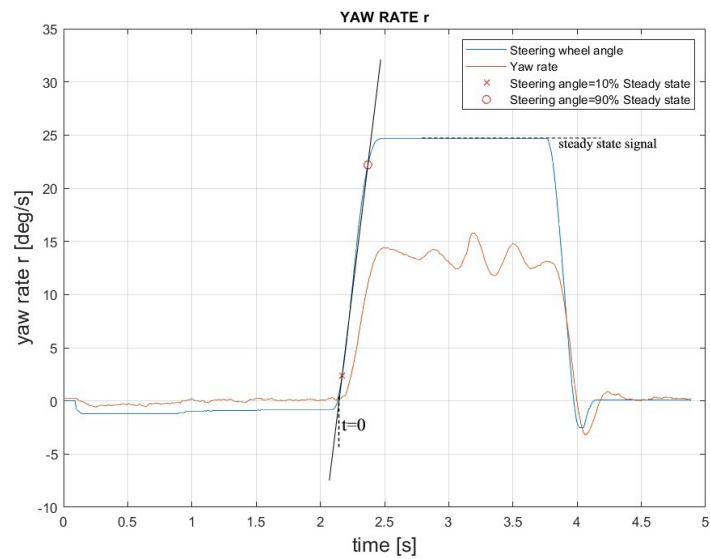


Figure 23: system response delay- step steer manoeuvre

Steering inertia is an important parameter impacting on the response of the system, since it impairs the way the vehicle retrieves its equilibrium condition, slowing the response to get back on straight trajectory. Moreover, the steering inertia increases the oscillatory behaviour of the system and, if damping component were not present, would produce a non-stable system.

## 1.4. VEHICLE LONGITUDINAL DYNAMICS

Vehicle longitudinal dynamics involves all what concerns the resistance to motion. When travelling on a level road along a straight direction, two most resistance forces must be overcome by the vehicle: the aerodynamic force and the rolling resistance. When the road is not flat but has a certain inclination, also the climbing resistance must be considered.

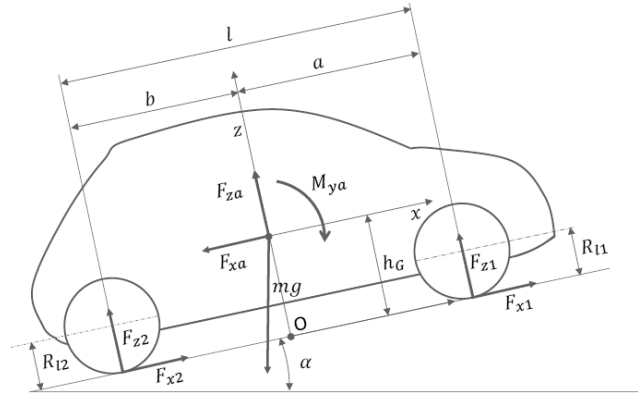


Figure 24: vehicle longitudinal dynamics reference system

- Rolling resistance

It is the force resisting to motion when a deformable body rolls on a surface. It is given by the energy dissipation due to slippage between wheels and road. It is known from the literature <sup>[1]</sup> that rolling resistance is function of the speed as:

$$F_{roll} = \sum_{i=1}^4 F_{zi}(f_0 + KV^2)$$

Where  $F_{zi}$  is the vertical force acting on each wheel while  $f_0$  and  $K$  are coefficient function of the specific tyre. The term  $(f_0 + KV^2)$  is the rolling coefficient  $f$ .

Vertical force can be expressed as function of the lift coefficient  $C_z$  and of weight force, so rolling resistance will become

$$F_{roll} = \left( mg \cos(\alpha) - \frac{1}{2} \rho C_z S V^2 \right) \cdot f$$

- Climbing resistance

It is the resistive force acting against the vehicle due to the surface to be inclined by  $\alpha$  angle. This will lead to a non-vertical weight force to be overcome.

$$F_{climb} = mg \sin(\alpha)$$

- Aerodynamic resistance

According to the vehicle front dimension  $S$  and to the velocity of motion, the aerodynamic will produce a resistive force against the direction of motion.

$$F_{aero} = \frac{1}{2} \rho C_x S V^2$$

Where  $C_x$  is the drag coefficient,  $\rho$  the density of the air and  $V$  the relative velocity of the vehicle with respect to the air.

It is important to notice that as vehicle speed increase, so will do the aerodynamic force in a quadratic way, becoming the higher contribution to the motion resistance, especially for light vehicles.

The global formulation of the resistance force can be so written as:

$$F_{res} = F_{roll} + F_{climb} + F_{aero}$$

$$F_{res} = \left( mg \cos(\alpha) - \frac{1}{2} \rho C_z S V^2 \right) \cdot f + \frac{1}{2} \rho C_x S V^2 + mg \sin(\alpha)$$

Generally, in literature this force can be found rewritten in order to highlight the dependence of velocity:

$$F_{res} = A + BV^2 + CV^4$$

Where usually the last term  $C$  is neglected since impacting only at high speeds or in vehicles showing strong negative lift.

The power needed for motion at constant speed can be obtained by multiplying this resistance force by  $V$ .

$$P_{needed} = AV + BV^3 + CV^5$$

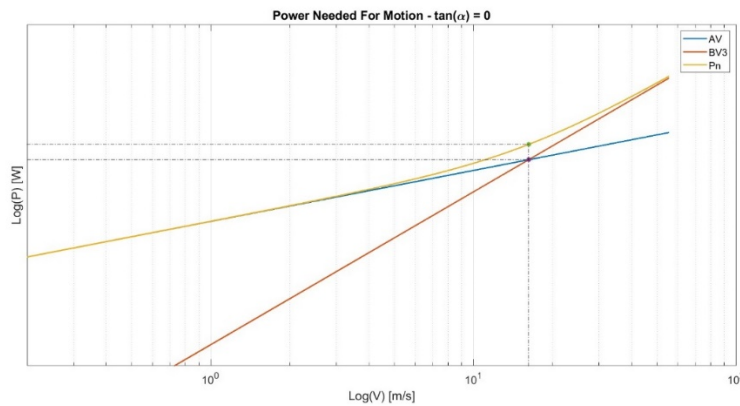


Figure 25: Power needed for motion on a flat road

When the slope is null, so if the vehicle is travelling on a flat road, the abscissa of intersection between AV and BV<sup>3</sup> is the characteristic speed  $V_{char}$ , while the ordinate represents half of the characteristics power  $P_{char}$ .

$$V_{char} = \sqrt{\frac{A}{B}} \quad P_{char} = 2A \sqrt{\frac{A}{B}}$$

The available power at the wheels must be higher than this  $P_{needed}$  in order to move the vehicle.

It can be evaluated starting from the power generated by the engine  $P_e$  taking into account the efficiency of the driveline  $\eta$ :

$$P_{avail} = P_e \cdot \eta_t$$

Anyway, the maximum power that can be transmitted to the ground is limited by the friction coefficient  $\mu_{ip}$  of the  $i$  driving wheels.

$$P_{max} = V \sum_i F_{zi} \mu_{ip}$$

## 1.5. STANDARD MANOEUVRES FOR LONGITUDINAL DYNAMICS

To control the vehicle longitudinal dynamics, the most common test performed is the so-called Coastdown manoeuvre.

It consists of driving the vehicle on a straight road up to a defined speed, placing the neutral gear and letting it slow down until reaching the stop, or a given speed, without pressing the brake pedal.

This manoeuvre is usually performed to evaluate the parameters of the vehicle that contribute to composing the global resistance to motion, such as aerodynamic resistance and mechanical one. Rolling resistance coefficient is usually defined with this test too.

## 2. VEHICLE SENSORS SETUP FOR TESTING

To correctly analyse the dynamics of a vehicle under test, standard manoeuvres as those described above must be performed and signals collected, in order to define the response of the system under given excitation.

Sensors are widely used for this purpose in the automotive field, allowing different signals to be acquired by electronic means and used by post processing tools. In this chapter an overview on the most important sensors is given, focusing on their technology and on the automotive application.

An explanation of the general layout of how the sensors are placed on the vehicle body will be provided too, integrated by the description of the acquisition process. The latter can be performed by CAN bus, analog or digital networks depending on the type of sensor: an overview of the differences between them can be found in what follows.

### 2.1. SENSORS

Sensors are devices that transform variations of input non-electrical physical quantities into electrical signals, intended as variations of electrical quantities suitable to be acquired and processed by electronic means.

Since most of the quantities of interest in the automotive field are non-electrical, sensors are essential parts of almost any automotive electronic control system.

In particular, as seen above when recalling vehicle dynamics basics, main parameters needed to characterize the dynamic of a vehicle are:

- Longitudinal, lateral, vertical acceleration
- Angular velocity and acceleration around  $x,y,z$
- Side slip, yaw, pitch and roll angle
- Steering angle and steering moment
- Brake pedal force and *travel* pressure
- Vehicle speed

These quantities need to be acquired by sensor mounted over the vehicle body. The main sensors allowing those measures are here listed and then shortly described.

- Accelerometers
- Inertial Measurement Unit
- Optical sensors
- Load cell
- Steering angle, torque and speed sensor
- Linear position sensors

### 2.1.1. ACCELEROMETERS

Information about linear acceleration along the three axis of the vehicle is generally provided by the Inertial Measurement Unit but can also be retrieved by a triaxial accelerometer of the MEMS (Micro-Electromechanical Systems) technology. An accelerometer is a sensor that senses axial acceleration and converts it into a usable output signal. The operating principle is based on the presence of two metal plates connected by a spring of known rigidity constant. One plate is integrated in the body frame while the other one is suspended and subjected to an inertial force  $F = m \cdot \ddot{x}$ , where  $m$  is the mass of the suspended plate while  $\ddot{x}$  the acceleration in  $x$  direction. Such a force will induce a change in the distance between the plates depending on the rigidity constant of the spring.

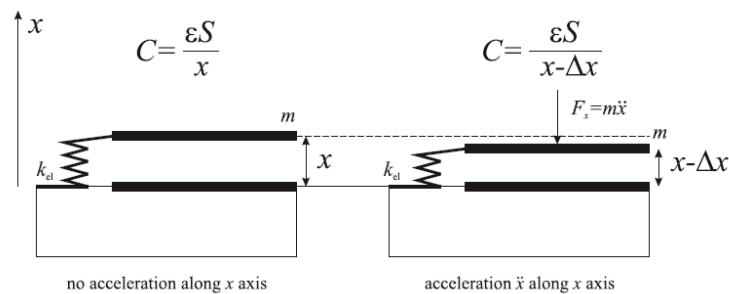


Figure 26: MEMS accelerometer structure [4]

The capacitance between the two metal plates can be expressed as  $C = \frac{\epsilon S}{x}$  where  $\epsilon$  is the permittivity of the dielectric present between them and  $S$  is the surface. Due to the inertial force, the distance between the plates will change and so their capacitance. Through a capacitive bridge structure driven by a square wave signal, it is possible to

convert the change in capacitance into a detectable signal of voltage, proportional to the vehicle acceleration.

The signals coming from this sensor are acquired in analog system.

The accelerometer used during vehicle testing in this study has the following characteristics:

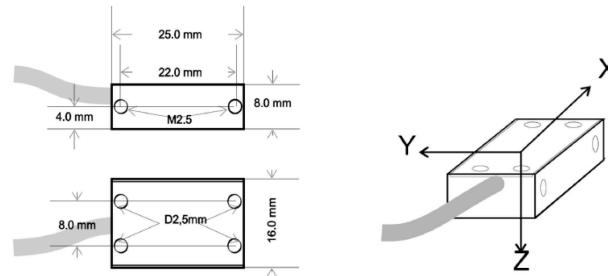


Figure 27: accelerometer technical data [3]

Characteristic	value
Range x axis	$\pm 5g$
Range y axis	$\pm 5g$
Range z axis	$\pm 10g$
Accuracy	1%
Cut off frequency	100 Hz
Output voltage	0-5 V
Signal at 0g	$2.5 \pm 0.05$ V
Acquisition	analog
Sampling frequency	100 Hz
delay	negligible

Table 1: accelerometer technical data[3]

### 2.1.2. INERTIAL MEASUREMENT UNIT

An inertial measurement unit is a device that consists of three accelerometers and three fibre optical gyroscopes, which grip an orthogonal, gyro-fixed coordinate system, firmly connected to the vehicle-fixed one.

Every movement referring to a fixed road system of coordinates is registered by the gyroscopes and represents the vehicle movement.

The following parameters are the measuring output:

- Accelerations ( $a_x, a_y, a_z$ )
- Angles ( $\alpha_x, \alpha_y, \alpha_z$ )
- Rotational increments ( $\omega_x, \omega_y, \omega_z$ )

The three accelerations  $a_x, a_y, a_z$  and the three angular velocities  $\omega_x, \omega_y, \omega_z$  are transmitted directly in the horizontal coordinate system and are output either as analog data or via the CAN bus.

The angles of rotation, instead, are obtained by integrating the rotational increments measured by the fibre optical gyroscopes and compensating for the system errors such as gyroscopic drift or calibration factor. Vehicle speed is also considered while integrating. Signals coming from this sensor are acquired via CAN network. The inertial measurement unit used during vehicle testing in this study has the following characteristics:

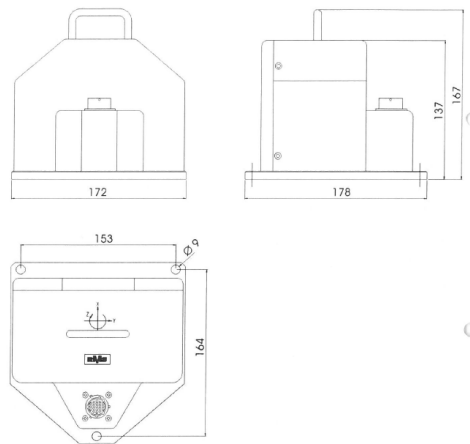


Figure 28: Inertial measurement unit technical data [3]

Characteristic	value
Power supply	10-28 V
Power	35 W
Supply current	3A
Start-up time	3 min
Acquisition	CAN bus
Sampling frequency	200 Hz
Baud Rate	500 kBaud

Table 2:: Inertial measurement unit technical data [3]

### 2.1.3. OPTICAL SENSORS

For a complete analysis of the rolling behaviour of the vehicle, the variation of distance from ground of fixed points on the body should be considered. Laser height-sensors are used for this purpose allowing non-contact distance measurement.

These sensors are based on the principle of optical triangulation. A visible red laser is focused on the road surface and the reflected light is collimated on a linear CCD array <sup>(1)</sup>.

The output of the sensor is proportional to the measured height.

For the studies here reported, two sensors have been used with the characteristics reported below, positioned respectively on the driver and on the front passenger door.

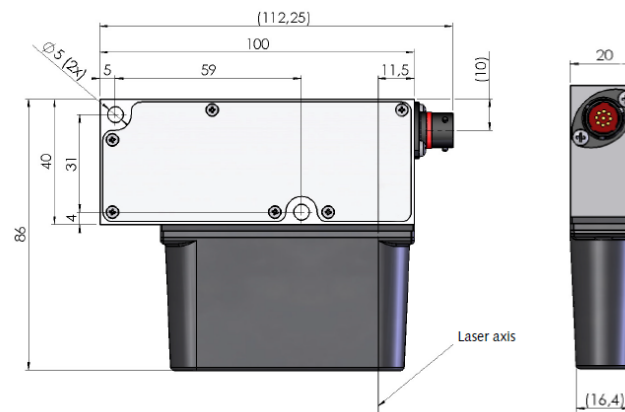


Figure 29: Optical sensor (laser) technical data [3]

Characteristic	value
Measurement range	125-625 mm
Resolution	0.2 mm
Linearity deviation	$\pm 0.2$ %
Sampling rate	250 Hz
Light source power	<5 mW
Light source wave length	660 nm
Signal output	0-10 V
Baud Rate	1 MBaud

Table 3: Optical sensor (laser) technical data [3]

(1) Charge coupled device: integrated circuit formed by a row, or a grid, of semiconductor elements capable of accumulating an electric charge proportional to the intensity of the electromagnetic radiation that hits them. By sending a timed sequence of pulses to the device, an electrical signal is obtained at the output thanks to which it is possible to reconstruct the matrix of pixels that make up the image projected on the surface of the CCD itself. The pixel number between the principal point of the CCD and the laser spot projected from the laser project varies according to the distance of the targeted object.

For what concerns vehicle speed and slip angle, a non-contact optical sensor has been used in the development of this thesis, installed on the front of the vehicle.

It is composed by a lamp and is able to measure the angle between vehicle axis and vehicle trajectory. Integrated accelerometers enable the determination of additional measurands like longitudinal and transverse acceleration of the vehicle. Pitch, roll and rotation around vertical axis of the vehicle can be measured too thanks to integrated angular rate sensors. Signals coming from optical sensors are acquired via CAN network.

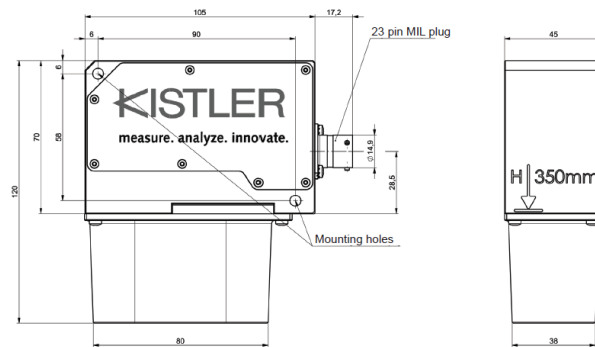


Figure 30: Optical sensos technical data [3]

Characteristic	value
Speed range	$\pm 0.1 - 250$ km/h
Distance resolution	$\leq 1$ mm
Measurement accuracy	$< \pm 0.2$ %
Angle range	$\pm 30^\circ$
Angle resolution	$< \pm 0.01$ %
Measurement accuracy angle	$< \pm 0.2^\circ$
Sampling frequency	250 Hz
Sampling rate	250 Hz
Baud rate	1 MBaud
Analog output	-10;10 V
Calibration distance	200 m

Table 4: Optical sensos technical data [3]

### 2.1.4. LOAD CELLS

Load cells are force sensors used in automotive testing to collect the braking force exerted by the driver. According to the force measured the sensor put out an analog signal independent on the angle of activation force.

These sensors are based on the piezoresistive effect and composed by a metal body to which strain gauges are secured. When force is exerted on the load cell, the elasticity of the metal induces the body to be deformed as well as strain gauges. The change in shape results in a change in resistance and can be measured as voltage. Since the change in resistance measured by a single strain gauge is extremely small, usually many of them are connected in a specific circuit allowing the change in resistance to become as high as needed to be measurable. This circuit is known as Wheatstone Bridge.

With this configuration the change in voltage is proportional to the amount of force applied to the cell, so allows to retrieve it from the sensor's output signal.

Load cell signals are acquired in analog way.

The load cell used in the tests reported in this has the characteristics reported below.

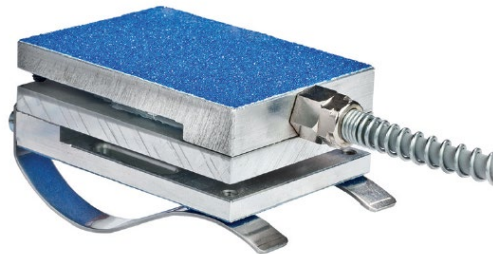


Figure 31: Load cell technical data [3]

Characteristic	value
Measurement range	0-1500 N
Accuracy	±5 %
Output range	0-5 V
Overload	1800 N
Sampling rate	100 Hz

Table 5: Load cell technical data [3]



<i>Characteristic</i>	<i>value</i>
<i>STEERING MOMENT</i>	
<i>Measurement range</i>	±50 Nm
<i>Accuracy</i>	±0.15 %
<i>Linearity deviation</i>	±0.15 %
<i>Sampling rate</i>	250 Hz
<i>Baud rate</i>	1000 kBaud
<i>Signal output</i>	-10 ; 10 V
<i>STEERING ANGLE</i>	
<i>Measurement range</i>	±1250 °
<i>Accuracy</i>	±0.1 %
<i>Resolution</i>	0.015°
<i>Sampling rate</i>	250 Hz
<i>Signal output</i>	-10 ; 10 V

Table 6:Steering angle, torque and speed sensor technical data [3]

### 2.1.6. LINEAR POSITION SENSOR

Potentiometers are linear position sensor devices used in automotive field during testing. Due to their simplicity and versatility can be employed to measure different variables as, for example, the brake pedal travel. These sensors convert information about the linear position of a moving element into an electrical signal and include a wire resistor connected to the moving element via a sliding contact allowing the linear motion of the cursor along the length of the resistor.

When a constant supply voltage  $V_{DD}$  is applied at the two terminals of the wire resistor, the voltage between the cursor and the negative voltage of the source will be given by the voltage divider rule and change depending on the position of the cursor  $x$  according to Second Ohm's Law, where  $\rho$  is the wire resistivity,  $l$  the length and  $S$  the section:

$$R_1 = \frac{\rho l}{S} \quad R_2 = \frac{\rho(l-x)}{S} \quad V_x = V_{DD} \frac{x}{l}$$

In this way, output voltage will linearly depend on the position of the cursor.

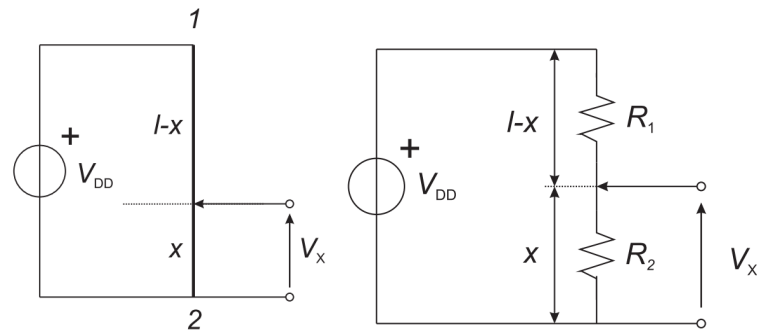


Figure 33: Linear position sensor [4]

Signals coming from these sensors are acquired in analog way and can be assumed to be delay-free. In the study of this thesis, a potentiometer with the characteristics reported below has been used:

Characteristic	value
Measurement range	0-75 mm
Accuracy	$\pm 0.7\%$
Linearity	$\leq \pm 0.5\%$
Resistance	$5 \pm 20\% \text{ K}\Omega$
Sampling rate	100 Hz

Table 7: Linear position sensor technical data [3]

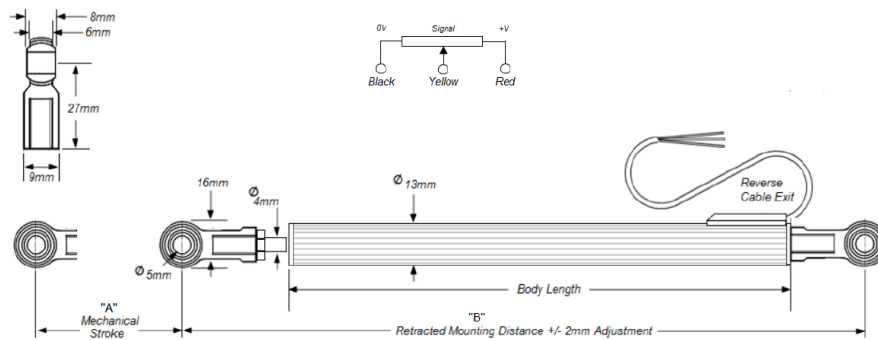


Figure 34: : Linear position sensor technical data [3]

## 2.2. GLOBAL LAYOUT

During road testing, the vehicle is usually equipped with all or many of the sensors described above. Depending on their functionality, they may have to be mounted in a specific place or can have a variety of possibilities.

In this section of the project, an overview of where usually these sensors are placed is given, starting from the layout used during the road testing session of the hybrid supercar in analysis.

The images here reported refers to a different vehicle, but the placing of the sensors faithfully reproduces the one used for the studies of this thesis.

In the scheme below, an illustration of how the vehicle is equipped with sensors is given.

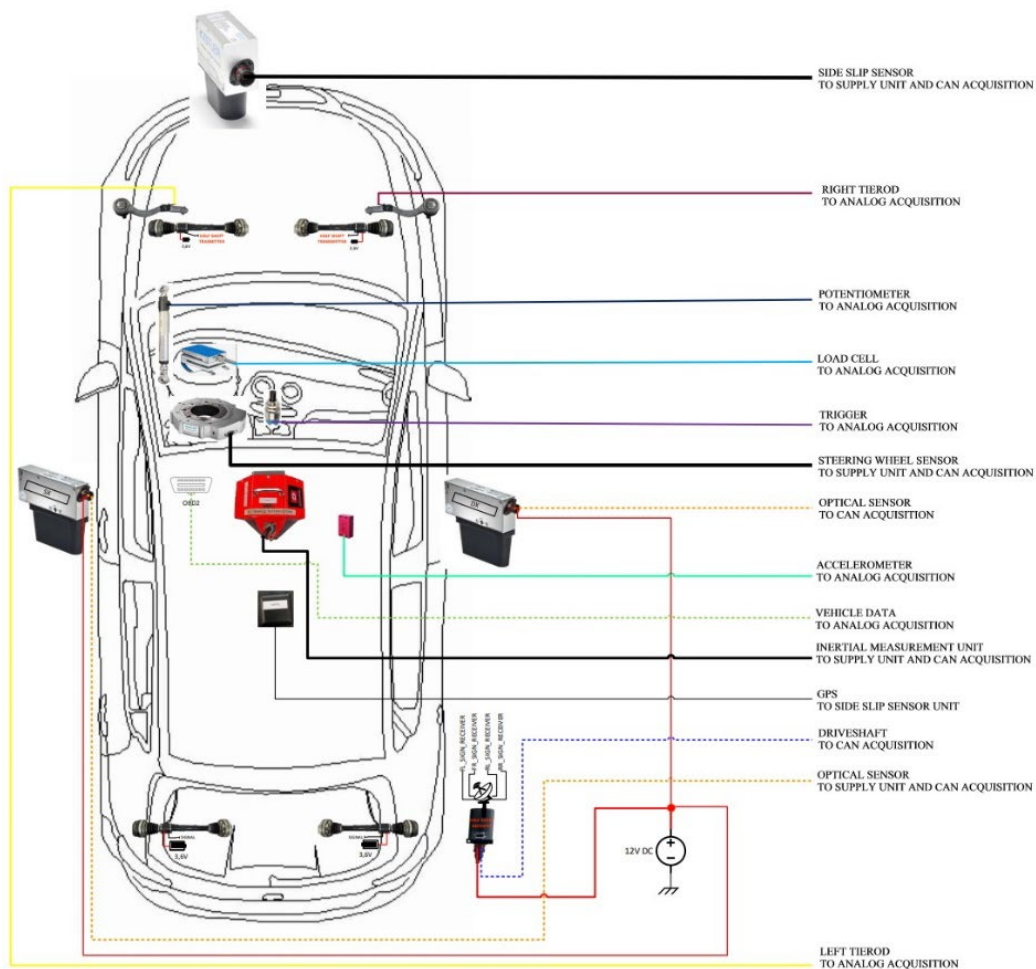


Figure 35: Global layout of vehicle sensors positioning [3]

In particular, it can be seen that:

- Optical sensor for distance from ground are positioned on the driver and passenger doors at a height of around 30 cm, in order to analyse the signals and evaluate the rolling behaviour of the car
- Optical sensor for side slip angle and vehicle slip is positioned on the front of the vehicle, at a distance of around 35cm from ground.



*Figure 36: Optical sensors for vehicle height (left) and side slip angle (right)*

- Steering angle, torque and angle rate sensor is placed on the steering rack, substituting the original steering wheel or integrating the two.



*Figure 37: Steering torque sensor*

- Load cell to evaluate braking force is placed on the brake pedal so that the driver will directly apply his force on it.



*Figure 38: Load cell on brake pedal*

- Linear position sensor is placed behind the brake pedal and can slide measuring the brake pedal travel.



*Figure 39: Potentiometer*

- Inertial measurement unit to evaluate accelerations, angles and rotational increments should be placed as close as possible to the vehicle centre of gravity and when not possible, anyway positioned in a fixed reference system. A usual place chosen is behind the rear seats.



*Figure 40: IMU system positioning*

- Accelerometer can be used as feedback comparing the collected signals with the ones coming from IMU sensor. Usually, this mems accelerometer is placed in the seat guide to check for passenger comfort or over the IMU to check correctness.

All the signals collected with this configuration will be referred to the local reference frame of each sensor so, to be analysed, must be properly corrected and translated to the vehicle centre of gravity during the post processing phase.

### 2.3. DATA COLLECTION

All the signals coming from the sensors on the vehicle are collected through a data acquisition system, in charge to acquire both analog and CAN lines.

In this project the Dewe-43A device has been adopted, produced by *Dewesoft company*. It includes 8 analog input channels, 8 digital input channel and 2 CAN bus input channels. It has a self-synchronizing system with a precision of 1 ms.

Connecting this device to a personal computer it is possible to directly view and record the desired variables during the analysis or road test sessions.

The configuration of each channel is possible by importing the sensor database in the software, setting the important parameters of each one, as sampling frequency or Baud Rate.

It is also possible to activate an antialiasing filter but usually this function is avoided, preferring the filtering in post-processing phase.



Figure 41: Data acquisition system [3]

The software tool used for the acquisition is *DewesoftX*.

It allows to see real-time the trend of the values collected and to directly plot the desired graphs in post-processing. Signals can be exported in many formats to be processed in software as Matlab or Excel.

The environment chosen for the aim of this thesis to reconstruct dynamics behaviour of the vehicle has been *Matlab* by Mathworks company, with the help of Simulink tool.

### 3. REGENERATIVE BRAKING REVERSE ENGINEERING

The chapters above have been focused on defining the procedure to be followed to prepare a vehicle for road testing and to acquire data from the all the sensors and from vehicle data network.

In this third chapter, a description of the main components of a hybrid vehicle is provided, analysing advantages and limits. First of all, an overview of the vehicle architecture is given.

The following ones, instead, are dedicated to the analysis of the data collected during vehicle road testing on which this thesis is based on, performed by *Danisi Engineering* drivers in December 2021.

#### 3.1. CASE STUDY: PLUG-IN HYBRID VEHICLE LAYOUT

The vehicle analysed for this study is a Plug-in Hybrid Electric Vehicle (PHEV) supercar. Being plug-in hybrid, the main characteristic is that the on-board energy source can be recharged from the grid, leading to have a large contribution of the electrified powertrain and long electric drivability range. In this case, the vehicle is equipped with a battery of 26 Ah capacity. More details are reported below. Based on the following scheme, the vehicle studied can be classified as Full Performance parallel hybrid. As *parallel hybrid* a system in which ICE power flux and electrified power flux are separated is intended. Moreover, a great advantage of parallel hybrid with respect to the series one is the capability to drive the vehicle in pure electric mode, decoupling the two power sources.

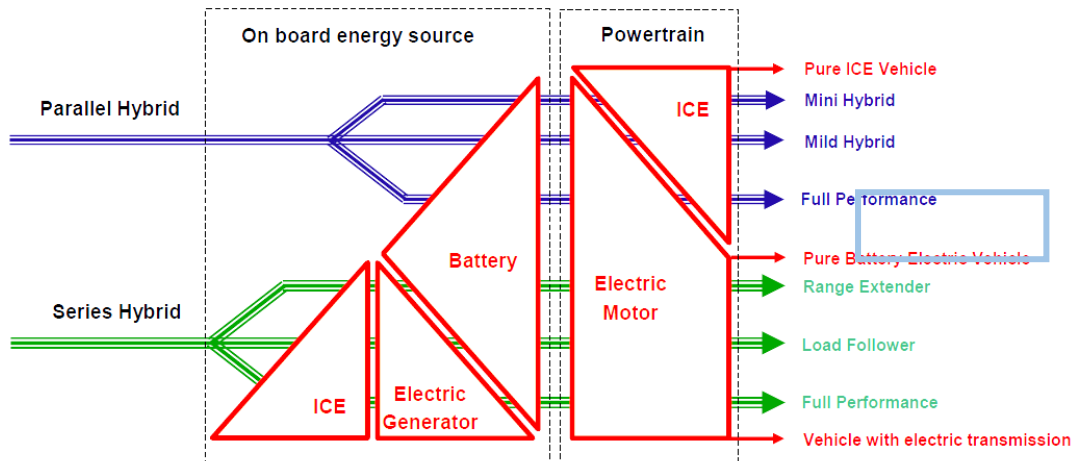


Figure 42: Hybrid classification [6]

The powertrain of the vehicle under test is composed by a traditional internal combustion engine placed on the rear part of the vehicle, coupled with three permanent magnet DC brushless electric motors:

- Two of radial flux type are placed on the front axle, in P4 position. They are in charge of providing front wheel drive traction when the vehicle is set in electric drive, while cooperate with ICE to set up an All-wheel drive traction when required. They can supply up to 85Nm and 100 kW each.
- An axial flux one is placed in P1 position, close-coupled with internal combustion engine before the 8-speed dual clutch transmission. It has a disc-shape design, with very small thickness due to the small displacement available. This rear motor can supply up to 260 Nm and 160 kW.

Each electric motor has a dedicated inverter, in charge of converting DC current in AC current, and a dc/dc converter to decouple the voltage on the battery side from the one on motor side.

To better understand the positioning of the electric motor, refer to the diagram below, showing the common classification classed P-method.

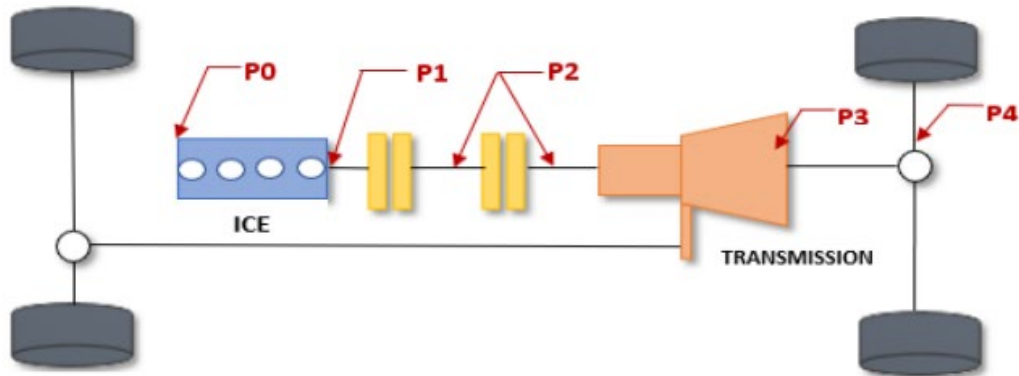


Figure 43: e-traction classification: P method [8]

The machine in P1 position is connected with ICE directly with the crankshaft: it is not possible to decouple electric motor and internal combustion engine thus it can not be used during pure electric drive and it is seldomly used for regenerative braking since torque losses occur.

The machines in P4 position are completely decoupled from the rear axle transmission: they allow pure electric driving and energy recovery during braking. Moreover, using two separate e-motors in P4 position enable the torque vectoring capability. Accelerating or braking the motors it is possible to change internal and external wheels speed according to cornering behaviour, or correct the trajectory for security reasons.

The global layout of the vehicle can be synthetized in the scheme below:

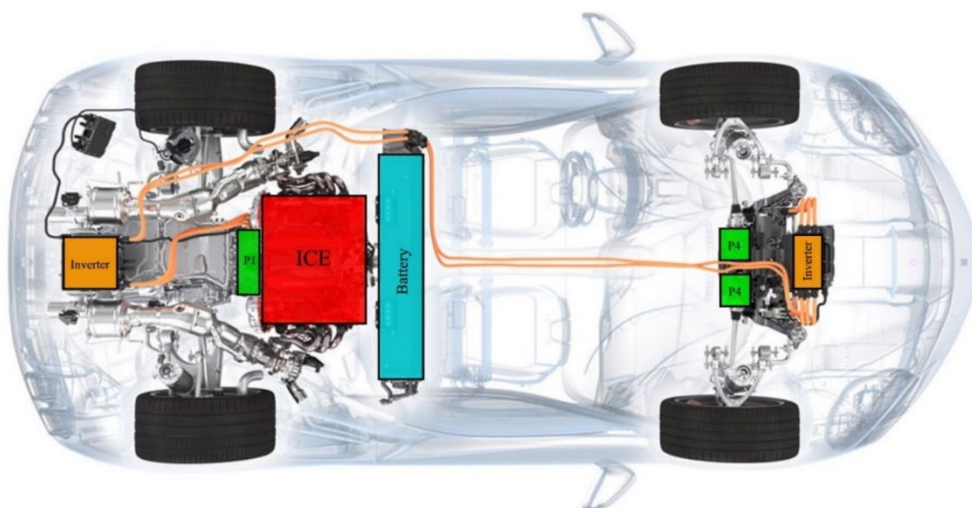


Figure 44: Vehicle powertrain layout [9]

The energy storage system is composed by a High Voltage Nichel-Manganese-Cobalt battery, placed rear the seats, with a nominal voltage of 350V.

The vehicle is equipped with an on-board charger, so can be recharged from the grid and can support up to 25km in full electric drive, with a very high power density. The battery has an integrated Battery Manage System BMS whose goal is to electrically control its charge and discharge, to continuously monitor cell temperatures and voltage and to provide parameters to the cooling system controller.

The front inverter is connected to the two P4 motors and is in charge of transforming the continuous current from the battery in an alternate three-phase current for e-Motors. It has an efficiency  $> 94\%$  and can manage voltages ranging 230-400 V.

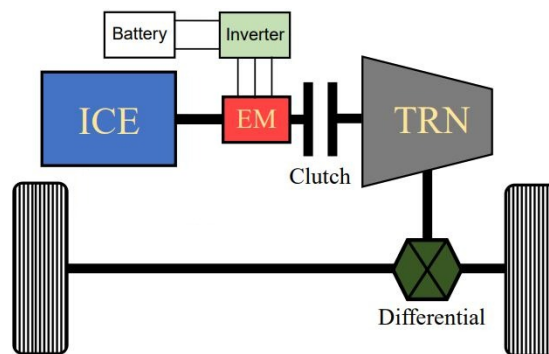


Figure 45:P1 architecture [5]

### 3.2. DRIVE MODES

The hybrid supercar considered in this thesis is equipped with a drive mode selector that gives to the driver the possibility to change some vehicle parameters according to the performances he wants to archive or to the powertrain he wants to utilize. It is possible to set a more racing setup when exploiting the maximum performance is needed or a normal one for everyday usage. For the purposes of this thesis, the powertrain selector is analysed, choosing the hybrid propulsion. An overview of the main tractive and braking layout is now given.

## 1. PURE ELECTRIC TRACTION

When the driver chooses the electric only drive mode from the selector, the internal combustion engine is shut down. All the tractive power will be supplied by the front electric motors, fed by the HV battery. The vehicle will be front wheel drive only. The power flow will be the one depicted below:

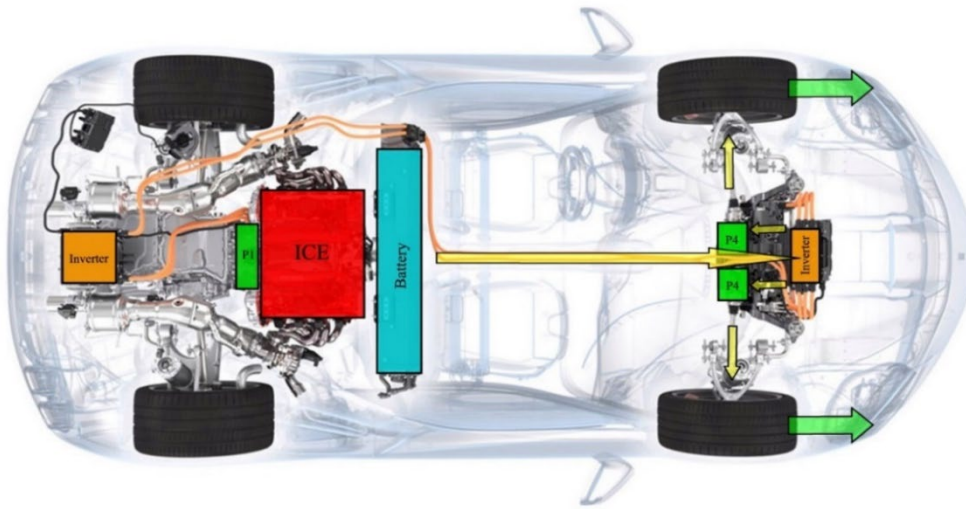


Figure 46: Pure electric traction layout [9]

## 2. HYBRID TRACTION

In case of hybrid drive selection, the default one, the two powertrain sources will cooperate providing an all-wheel drive traction. The HV Battery will supply the two P4 motors for the front traction and the P1 motor for the rear traction. The internal combustion engine will provide power on the rear axle too. The power flow will be the one depicted below:

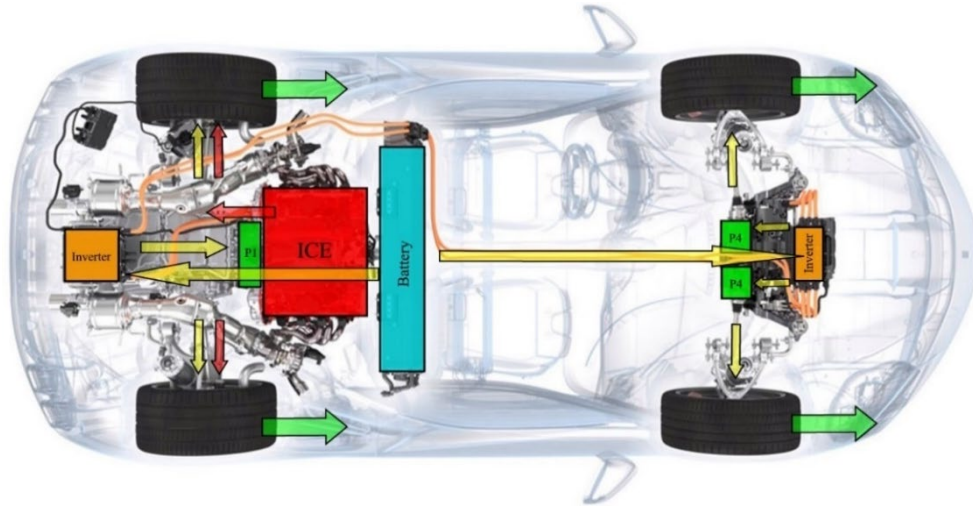


Figure 47: Hybrid traction layout[9]

### 3. REGENERATIVE BRAKING

Hybrid vehicles are designed such to optimize the energy flowing through the battery. Regenerative braking is one of the main contributors to this goal, allowing energy recovery when the vehicle is decelerating. Energy is stored exploiting kinetic energy from the road and transforming it into chemical energy to battery. This is done mainly thanks to the two front electric motors and partly from the rear one. The power flow will be the one depicted below:

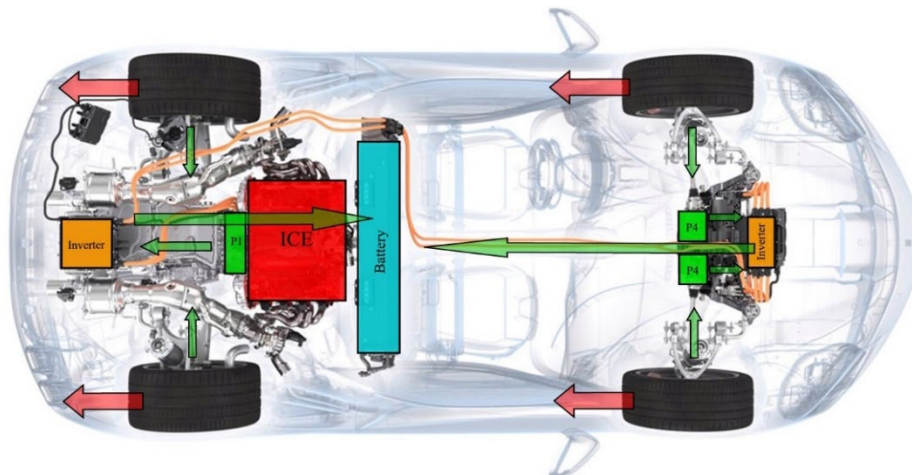


Figure 48: Regenerative braking layout[9]

### 3.3. REGENERATIVE BRAKING: THEORETICAL BACKGROUND

The adoption of electric powertrain is of main importance in increasing the efficiency of the system, contributing to the conversion to EV due to energy crisis and in paying attention to environmental issues.

Electric motors are efficient in converting electrical energy into mechanical energy extremely rapidly and as one of the main merits, have the capability of doing the opposite: converting kinetic energy back into electrical one. This capability allows to exploit regenerative braking, transforming the energy coming from the road into charge for the battery, thus increasing running distance.

Due to their ease of control, fast torque control and efficiency, brushless DC motors are usually employed for automotive electric and hybrid propulsion.

Moreover, exploiting braking capability from the electric machine, enable the possibility of using less the mechanical brakes thus reducing wear and increasing their life.

However, the absorbed capacity of regenerative energy is limited because of components size, as well as motor capacity, battery current limit or inverter characteristics. These limitations will be discussed in Chapter 3.3.2.

Due to these limitations, not only electric regenerative brakes can be employed to decelerate and stop the vehicle, but also mechanical brakes are needed. It is worth to recall that Anti-Lock Braking System (ABS) can be activated only by means of mechanical brakes: for this reason, in case of hard braking manoeuvres regenerative braking is not activated and only traditional braking is applied for safety reasons.

The coupling between the two braking systems can be designed in different ways:

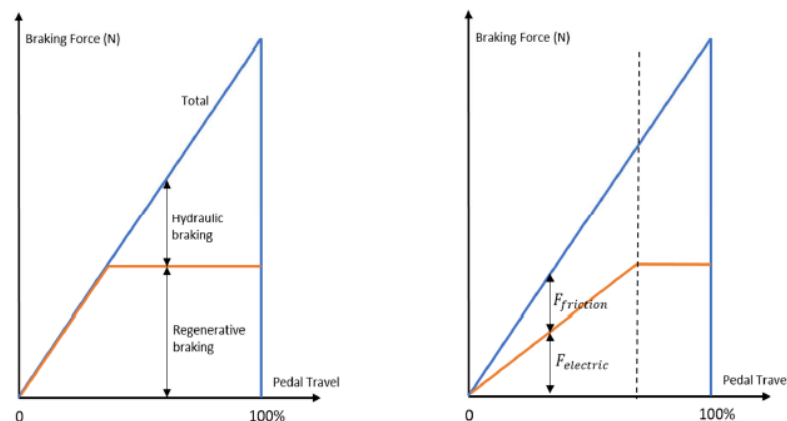


Figure 49: Split strategies of brake demand: series(left) and parallel(right) phasing [10]

- On *series* phasing strategy, the braking system is designed such to impose electric braking in the first part of braking pedal travel, and then mechanical braking intervention from the pedal travel threshold on, competing to reach total braking force demand.
- In the *parallel* phasing strategy instead, the two braking systems are simultaneously activated for each brake pedal travel percentage. There is no moment in which the electric braking is working stand alone.

This second strategy is the one applied to the vehicle under test for this paper.

According to the European Union legislation for braking systems in passenger vehicles, *UNECE Regulation 13H* <sup>[11]</sup>, the vehicle response in terms of driver's feel and deceleration must remain related to the driving situation and to the brake pedal position, being repeatable and remaining constant regardless of electric braking torque availability. For this reason, braking systems arranged for restore energy during braking events must always be designed as to have a control unit capable of modulating the mechanical braking force such to keep total braking force constant for a given pedal request.

These systems are called brake-by-wire: the braking pedal is no longer connected directly to brake traditional components as pumps, vacuum servos and master cylinder, but sensors and actuators are employed to control brakes by electronical means.

The amount of total braking force to be exerted is determined by the brake control unit according to the signals coming from sensors (wheels speed and pedal travel) and, according to split strategy adopted and to the deceleration target, the amount of electric and mechanical braking needed is determined.

### 3.3.1 ELECTRONIC BACKGROUND FOR ELECTRIC MOTORS

When discussing about the usage of electric motors as generators to restore energy to battery, it is worth to recall the basis behind the conversion of kinetic energy into electrical one, specifically applied on Permanent Magnets Brushless DC Motors.

Any time a charged particle moves inside a magnetic field, there will be a force acting on it, proportional to the particle charge, to the magnetic field strength and to the portion for which the velocity of particle is perpendicular to the field, according to Lorentz's law. This force will be in a direction perpendicular both to particle velocity vector and to magnetic field.

$$F = q \cdot \vec{E} + q \cdot \vec{v} \times \vec{B}$$

Where  $q$  is the particle charge,  $E$  the electrostatic field,  $v$  the particle charge and  $B$  the magnetic field.

This law find application in motors when discussing about current. Having a current  $i$  flowing through a wire of length  $l$  in a magnetic field, forces will result applied to the flowing particles, converting electric current into a mechanical motion.

$$F = i \cdot l \times \vec{B}$$

When current flows into a closed wire, the force will act letting the loop rotate half turn such to find equilibrium position in a point when forces are aligned and no momentum is present. The torque generated during the motion is proportional to the arm  $b$  of the forces, in this case assumed as the diameter  $d$  of the loop:

$$T = b \cdot \vec{F}$$

$$T = d \cdot (il \times \vec{B})$$

According to Faraday Law: if an external magnetic field going to the loop changes producing a change in the magnetic flux  $\phi$ , an electromotive force  $\varepsilon$  will be generated across the loop itself, such to have current flowing into it and resist to change of magnetic flux.

$$emf = \varepsilon = -\frac{d\phi}{dt}$$

The change in magnetic field can occur due to changes in magnetic strength or to change of direction between the current flowing in the loop and the field itself. This rotation is the primary way in which back emf is generated in motors.

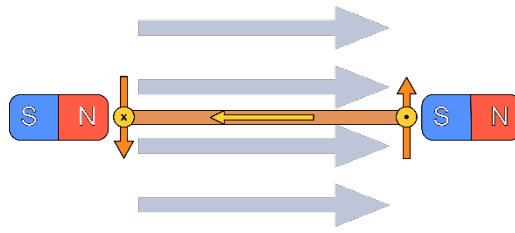


Figure 50: Coil in an external magnetic field with current flowing through and force applied

Torque is maximised when the coil is in line with the magnetic field, so when the magnetic field induced by the loop of wire is perpendicular to the external magnetic field, while it is zero when they are parallel.

To fix this issue, electric motors use multiple loops of wires, usually three with an offset of  $120^\circ$ , switching current path through them in a process called commutation. In this way, torque will be always produced in at least one of the three loops. The three loops are connected together such that current can flow through all of them, in order to always have positive torque.

Each coil is composed by  $N$  loops, so the torque produced by the motor is become proportional to

$$T = i l d \vec{B} N$$

$$T = i \cdot K_t$$

The current supply is the only variable that can be controlled, while all others are imposed by the manufacturer and can be summarized in the Torque constant  $K_t$ .

Therefore, the torque a motor can produce is only limited by the current flowing through it.

Schematizing the single phase of a motor as a resistive-inductive circuit, the voltage across this circuit is the difference between battery voltage and back emf.

The resistor is representing the heat losses along the circuit, the inductor is used to model the energy storage in the magnetic field induced by the coils, while the voltage generator represents the conversion of electrical energy into mechanical torque (back emf).

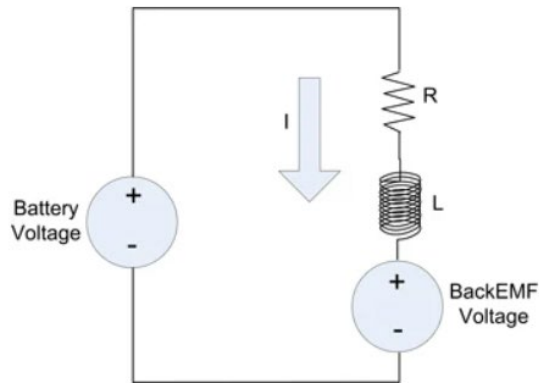


Figure 51: electric motor single phase equivalent circuit [14]

Knowing the expressions of mechanical power and electrical power, it is possible to equalize them, pointing out the equation for the back emf:

$$P_{elect} = i \cdot \varepsilon$$

$$P_{mech} = T \cdot \omega$$

$$i \cdot \varepsilon = T \cdot \omega = i \cdot K_t \cdot \omega$$

$$\varepsilon = K_t \cdot \omega$$

The back electromotive force is just function of motor angular velocity, proportionally.

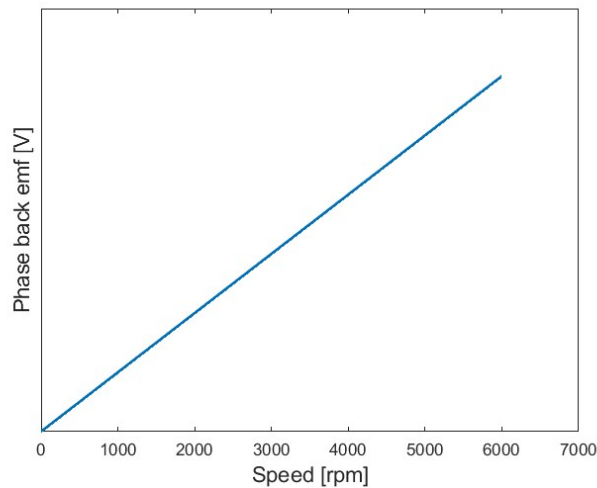


Figure 52: Dependence of back electromotive force on motor speed

As the back emf is opposite with respect to the supply voltage, the voltage across the resistive elements will drop when increasing the angular velocity, thus decreasing the current.

For this reason, there is a limit on angular velocity, given by the supply voltage divided by the resistance. Once reached that velocity, the motor can't turn any faster.

The recap:

Maximum torque produced by motor is imposed by the current flowing, while the maximum velocity is dictated by the supply voltage. The direction of rotation of the motor will determine the sign of the back emf, while the speed will determine the amplitude.

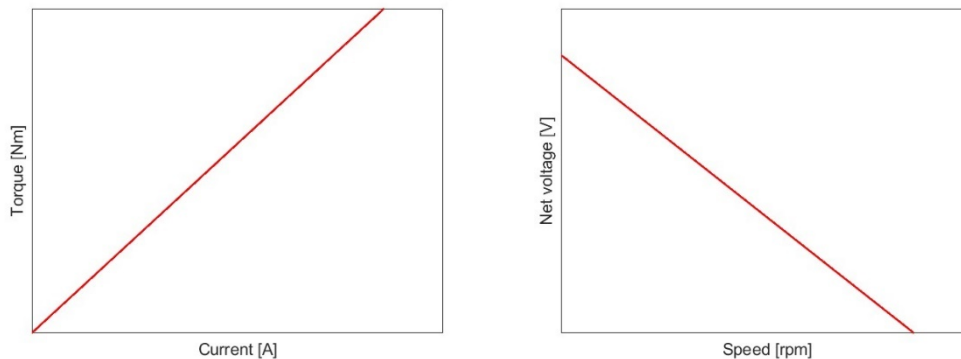


*Figure 53: Trend of torque as function of current*

*Figure 54: Net voltage in the cycle as function of motor speed*

### 3.3.2 BRUSHLESS MOTORS

Brushless motors, with respect to traditional brush motors, have the advantages of eliminating limits due to brush wear and of supporting high temperatures thanks to their higher capability to dissipate heat. This results in being capable of sustaining high currents without damaging the circuits, with the advantage of producing higher torque and mechanical power.

For these reasons, this electric motor's technology is very often employed in automotive applications and present in the vehicle analysed in this thesis work.

However, brushless motors require for a more complex control since commutation is obtained thanks to microprocessors and logics that replace the traditional brushes. For this reason, sensors and drivers are employed, increasing the cost. Coils are now placed on the stator, while the rotor is composed of permanent magnets, in one or more pole pairs.

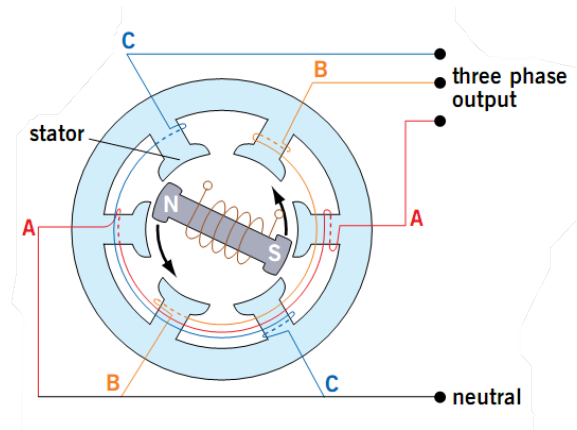


Figure 55: Brushless motor-generator layout [13]

Based on the Lawrence's law, the windings on the stator impose forces on the magnets, now free to rotate. The north side of the magnet will be subjected to a force pushing on the same direction of the external magnetic field, while the south will be subjected to an opposite force, resulting in a torque inducing rotation on the rotor [Figure 56].

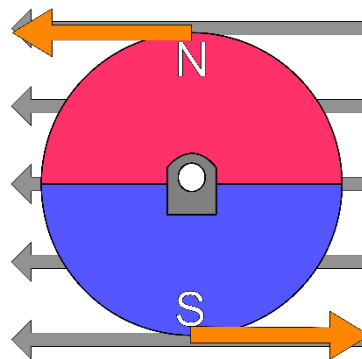


Figure 56: PM rotor in an external magnetic field (grey)

The torque acting on the rotor is maximised when the magnetic field induced by the magnets is perpendicular to the external magnetic field, regardless it is caused by another permanent magnet or by an induction due to current running through a wire.

For this reason, it is important that the external field induced by the windings on the stator continuously forms an angle of  $90^\circ$  with the rotor permanent magnet. This is done controlling the current flowing through the coils, through commutation.

### 3.3.3 BLDC MOTORS COMMUTATION

The current flowing through the coils can be modulated thanks to a circuit composed of three half bridges made by switches as in Figure 57, one for each phase of the stator.

The switches are mosfets of the Igbt (Insulated gate bipolar transistor) type, suitable for high power applications and of ease control.

Each switch is placed in parallel with a diode and can be turned on or off, connecting the phase to supply voltage or to ground. With a proper control, it is possible to set the correct path for current, in order to always induce a magnetic field such to produce the mechanical motion of rotor. The half bridge circuits allow to control individually each of the three phases. Usually one of them is connected to supply voltage and two to ground at each time.

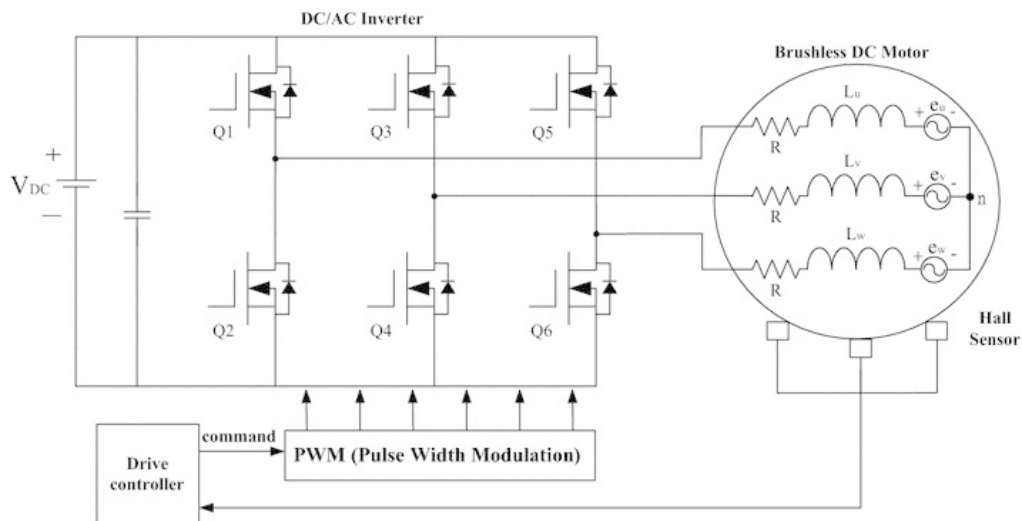


Figure 57: DC/AC converter with half bridge circuit architecture [12]

The control of the half bridge is driven by the signals collected by Hall sensors, placed around the rotor and sensing the position of this latter in order to decide when the current has to be applied in which phase, connecting the nodes to high voltage or to ground.

Moreover, not only the phases in which current must be driven can be decided but also the current modulation can occur, resulting in controlling the amount of torque produced.

The inductance inside the motor will act as a low pass filter for the current, making it change progressively and not instantaneously, allowing to modulate the amount of current flowing in the circuit by controlling the switching frequency of the mosfets.

This control is called Pulse with Modulation [17].

The PWM duty cycle controls the portion of the supply voltage from the battery that the motor is exposed to, also referred to as the effective voltage:

$$V_{eff} = R \cdot i + L \frac{di}{dt} + V_{emf}$$

The frequency of switching is decided based on the signals of the hall sensors and is transmitted to the switches through square wave signals.

The *duty cycle* is defined as the fraction of time in which the square wave that drives the switches is high, with respect to the whole switching period T.

$$D = \frac{T_{ON}}{T}$$

It is usually expressed as a percentage, varying between 0% (switch always off) and 100% (switch always on).

In the figure below the trend of the back emf on phases A, B and C is reported in red, green and blue respectively. It is possible to notice how PWM on the high side switches is performed on each phase when the emf is positive, while on the low side one diode is used to close the path for current.

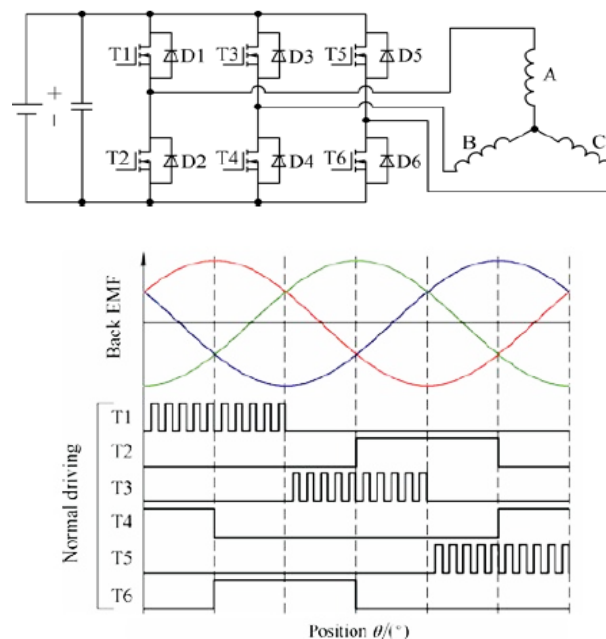


Figure 586 steps commutation – Traction [15]

By choosing the proper duty cycle, it is possible to modulate the effective voltage applied to the electric motor and so the current. Since torque is directly proportional to current flowing into the three phases according to the equations reported above, PWM is employed with the purpose of controlling the mechanical torque produced.

For what concerns braking manoeuvres, instead, the commutation of current in the three phases of the stator has not the purpose of creating the maximum tractive torque sustaining the rotor motion, but to decelerate it creating a resistive torque. The switching scheme can be changed in order to send the stored energy back to vehicle storage system, avoiding it to be dissipated into heat.

Due to the dependence of the regenerative torque on the battery charge, the electric braking is not always efficient: the maximum availability of energy to be recovered can be found in operating conditions including high vehicle speed and low battery state of charge. The reason is that the vehicle storage system allows an incoming power not always constant, but inversely proportional to the state of charge: the higher it is, the lower power can be transferred to the battery. In the following chapters a detail of the storage system adopted in this case study will be given. The back emf generated by the rotation of the rotor magnetic field is proportionally dependent on the motor speed according to the equations previously described, so higher at the beginning of the braking and progressively lower as the vehicle speed decrease. The current will be induced in the windings as a consequence, increasing as the electromotive force decrease.

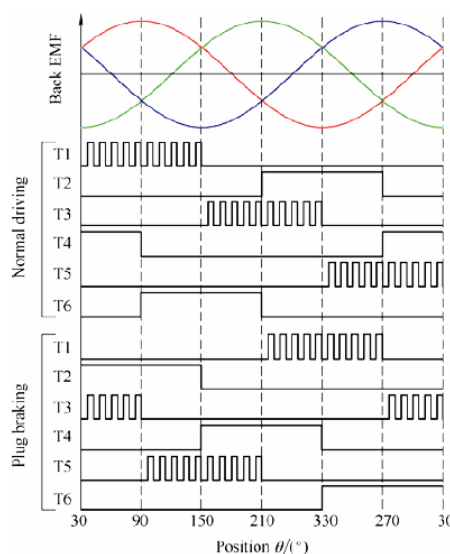


Figure 59:6 steps commutation – Braking [15]

In the figure above it can be seen as the switching scheme during braking is opposite with respect to the one performed during traction: PWM on the high side switches is performed on each phase when the back emf is negative, while on the low side one diode is used alternatively to close the path for current. This configuration is what can be defined “Plugging braking”, including a strategy to generate resistive torque in the motor to quickly decelerate the vehicle and dissipating the energy over a resistor, without caring about the regeneration.

In order to exploit energy storage, instead of wasting it on a resistor, regenerative braking requires for a specific strategy. The two main challenges to be accomplished are the alternatively connection of the 6-switches circuit to the motor and to the battery and the boost of the back emf.

To allow energy restoring into battery, the voltage at battery level is needed to be constant: for this reason, a kind of boosting is performed during the switching commutation, with functions equivalent to the ones of the circuit reported below

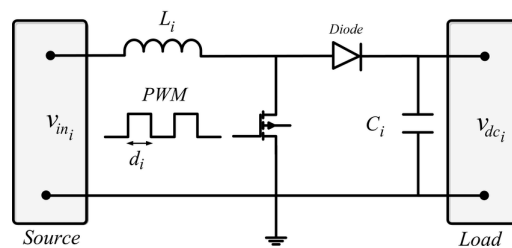


Figure 60: Boost converter circuit [12]

but realised by the inverter itself in two steps:

- *Storing phase*: the bottom switches are commanded to form a current waveform to produce the desired braking torque. The circuit is closed on two phases and the voltage increases due to the property of bldc motor inductances. In this phase the lower switch is on.

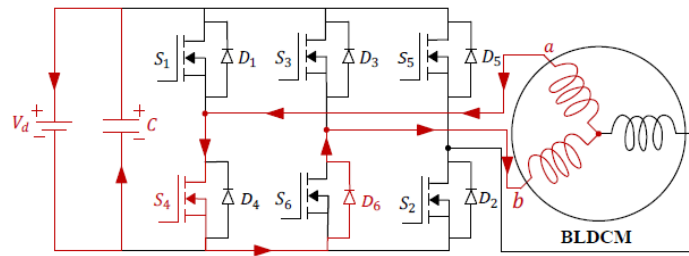


Figure 61: Storing phase of regenerative braking [16]

- *Energizing phase:* opening the switch the circuit closes on the battery with the current flowing through the two diodes and the energy can be used to charge the capacitor and transfer to battery. The voltage is high enough to allow battery charging and is given by the sum of the two phases emf and the voltage across inductances. In this phase the lower switch is off.

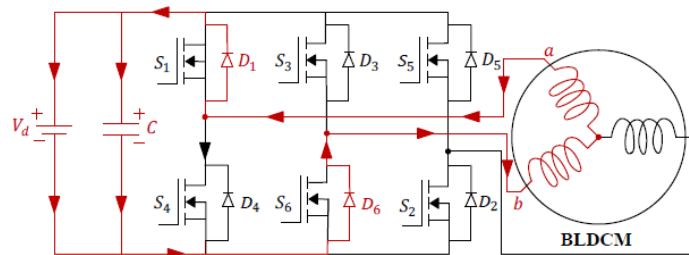


Figure 62: Energizing phase of regenerative braking [16]

The duration of one phase with respect to the other is what determines the increase of voltage in the inductance, of great importance in the regenerative braking:

$$V_L = L \cdot \frac{di}{dt}$$

For this reason, duty cycle of the PWM should be always determined by the control unit of the inverter such to let the storing phase last for the correct amount of time to guarantee enough boost. Since the emf value changes as the speed varies, so must the duty cycle do. In particular, during the braking event the electromotive force decreases, and the duty cycle must increase to keep voltage at battery level constant.

However, some limits are present when the back emf reaches low values: the inverter unit should act to let storing phase last for such a long fraction of the switching period to

increase the voltage to battery level, that the energizing phase will not be long enough to transfer the energy to battery. In this case regenerative braking would not be efficient and usually when the vehicle approaches a speed limit for which the electromotive forces fall below a threshold, the regeneration is interrupted and the switches are just operated to generate resistive torque, as in plugging strategy, but not storing energy.

The remaining energy due to induced current in the stator will be dissipated over the internal resistances of the circuit. To limit the amount of energy to be dissipated, the coupling with the mechanical brakes is of high importance.

For what concerns the vehicle in analysis, it was not possible to obtain specific information regarding the characteristics of the tractive system's components, due to privacy reasons. For the purposes of this thesis work, indeed, an assumption on the component's technologies was needed, and it is reasonable to say that the PWM control fits for this case.

## 4. DATA ANALYSIS

When dealing with reverse engineering, the main task is to focus on the available data and try to get the maximum information from them. When the amount of available data is limited, making good hypotheses may be needed, often confirmed or denied at the end of the process. For the purposes of this thesis, focused on the logics behind regenerative braking, the steps followed have been

- Collection of data during road testing
- Analysis of the specific braking manoeuvres
- Hypothesis and bibliography study of components characteristics
- Development and validation of a model for simulation

In particular, the manoeuvres analysed have been those defined as *Brake Step* and described in what follows, according to the company's standards.

### 4.1. BRAKE STEP MANOEUVRE

During road testing, one of the standard manoeuvres to characterize the braking system is the one called Brake Step. It is performed on a straight line and consists in taking the vehicle to a constant defined initial velocity, then release completely the accelerator pedal and press the brake one, keeping a constant pedal position until vehicle reaches full stop. In Figure 63 an example of the brake pedal history the driver should perform is reported.

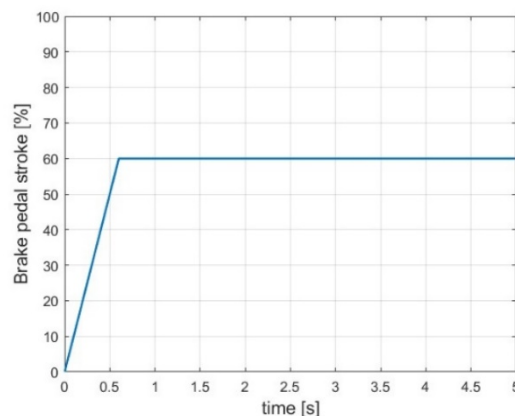


Figure 63: Drivel brake pedal history

Braking step is important since allows to characterize the braking response of the vehicle during straight manoeuvre regardless of factors that may affect it, such load transfer due to cornering or transients.

It is useful to check the repeatability of parameters of longitudinal dynamics, as the link between brake pedal stroke, vehicle speed and deceleration, if present.

For this purpose, the described manoeuvre should be performed at different initial velocities and different brake pedal stroke values.

When working with hybrid vehicles, usually equipped with a Brake-by-wire system, this kind of manoeuvre is useful to characterize braking control unit too, and the way in which braking torque is splitted between traditional and electric braking system.

In this chapter, the analysis of the road tests that brought to understanding the logics behind regenerative braking are illustrated. All the signals analysed have been collected with the procedure illustrated in Chapter 2, both from sensors with which the vehicle have been equipped and from the vehicle network.

In Figure 64, three tests recorded during road testing for this thesis are reported, in which the driver braking demand profile follow as much as possible a constant trend with the target values reported in Table 8. It must be specified that the signal collected from CAN network were referred to the real pedal stroke expressed in mm and have been normalized with respect to the maximum pedal stroke, whose value have been evaluated by the full braking tests.

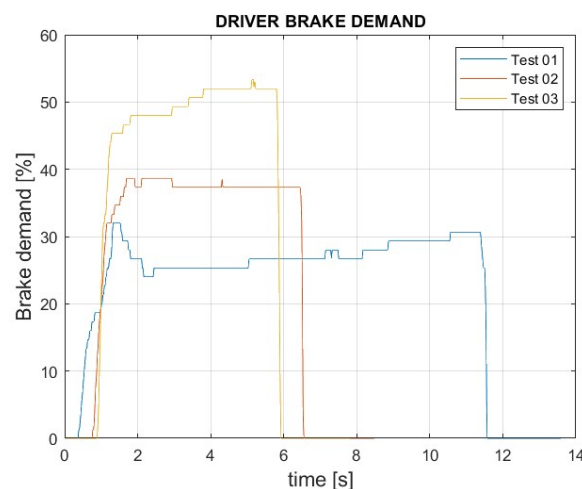


Figure 64: Brake step tests- driver brake demand

<i>Test</i>	<i>Average braking demand</i>
01	27%
02	37%
03	50%

Table 8: Driver brake demand

The acceleration profile and the trend of vehicle speed in the three tests in analysis can be seen in Figure 65 and Figure 66.

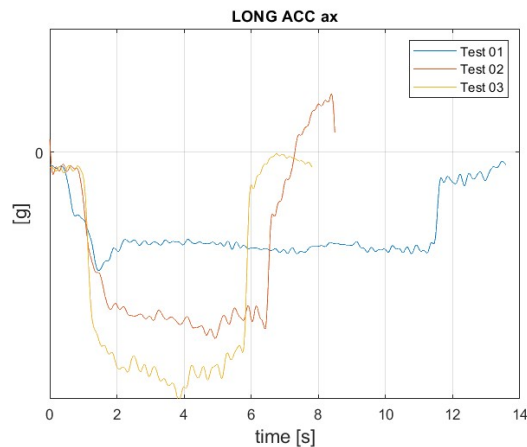


Figure 65: Brake step tests- acceleration

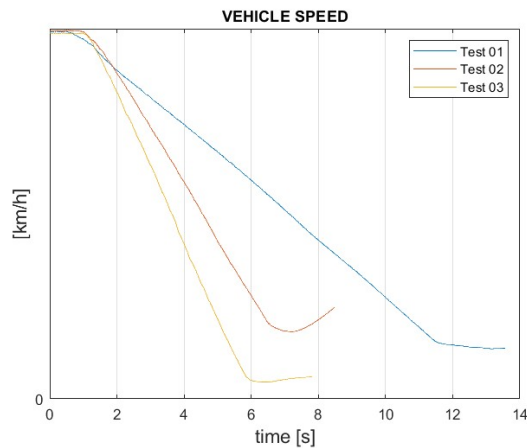


Figure 66: Brake step tests- vehicle speed

It is possible to notice as the vehicle follows, with a reasonable approximation, a constant deceleration during the whole manoeuvre. This assumption will be one of the most relevant one for the purposes of this thesis work, and the main goal to be reached by the simulation model developed. To confirm the correctness of this assumption, it must be considered that having a constant deceleration during braking is desirable in itself, to guarantee comfort and giving a better feeling to the occupants.

## 4.2. DECELERATION PROFILE EVALUATION

By analysing the available data collected during brake step manoeuvres, performed at different initial vehicle speed and brake pedal travel, and data from straight braking during whole track laps, it is possible to correlate the driver input parameters to the deceleration the vehicle performs, assuming it to be constant as seen in the previous paragraph.

To keep in consideration the link between resistive force to motion and vehicle speed, it is fundamental to pay attention to the coastdown manoeuvres, in which the brake pedal is completely released and the vehicle decelerate just due to the effect of inertia and aerodynamic forces. More details of this test have been illustrated in Chapter 1.5.

Reporting the analysed tests coming from track tests in an acceleration-velocity diagram, it is possible to obtain the pattern in Figure 67, where different colours refer to different values of driver brake demand. Values at 0% brake demand are retrieved from coastdown manoeuvres, while those at 100% from full braking ones.

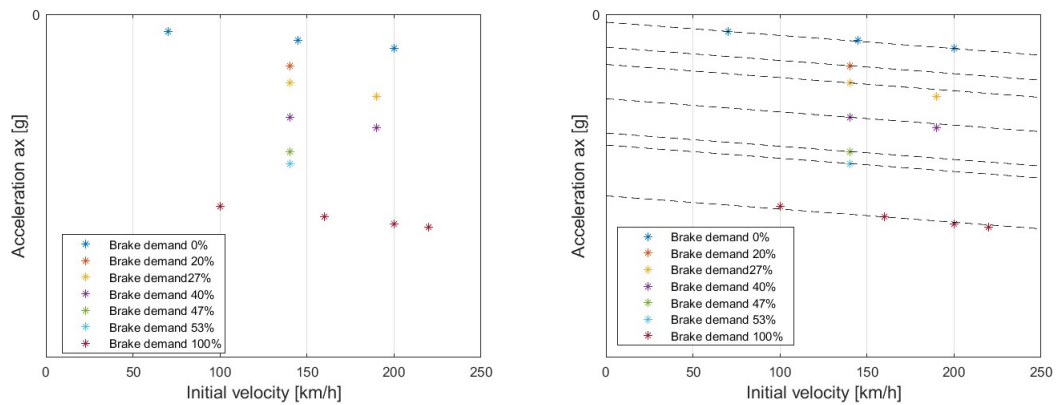


Figure 67: Deceleration pattern over tests(left)

Figure 68: Linear interpolation of deceleration profile(right)

As supposed from theoretical background, higher vehicle velocity corresponds to larger deceleration, since the aerodynamic contribution become important and scales with the square of the speed.

In order to get a complete table of the target deceleration as function of initial vehicle speed and driver brake demand, linear interpolation is used on the experimental values from coastdown tests, since considered as those less affected by driver accuracy in the

braking. Once obtained the coefficients of the straight line for 0% pedal stroke, the same gradient is transposed to all other values of brake request, obtaining the graph in (left) Figure 68.

The tests repeated more frequently with the same initial velocity and different brake requests are those at 140 km/h, for this reason the lines pass through those points with good accuracy.

In the same way, starting from the available data and from the coefficients of the line evaluated from linear interpolation, it is possible to build the whole scheme of target deceleration to be followed by the vehicle as function of pedal stroke and initial velocity, reported in Figure 69.

It is evident as the deceleration is larger when the initial velocity increases, due to aerodynamic contribution and to guarantee stopping of the vehicle in a safe distance. Moreover, the deceleration gradient is more sensitive to brake pedal demand in the central part of pedal stroke: it can be reasonably explained as a logic to have a better pedal feel and ensuring no strong deceleration to occur when the brake request is low, so to just slow down the vehicle.

Reconstructing this deceleration profile allows to understand the expected behaviour of the vehicle given the initial conditions, with the strong assumption to always have it constant, and to evaluate the stopping time and distance.

It is important to recall that this deceleration trend has been evaluated over manoeuvres of straight braking (brake step manoeuvres) and so fits only in those conditions.

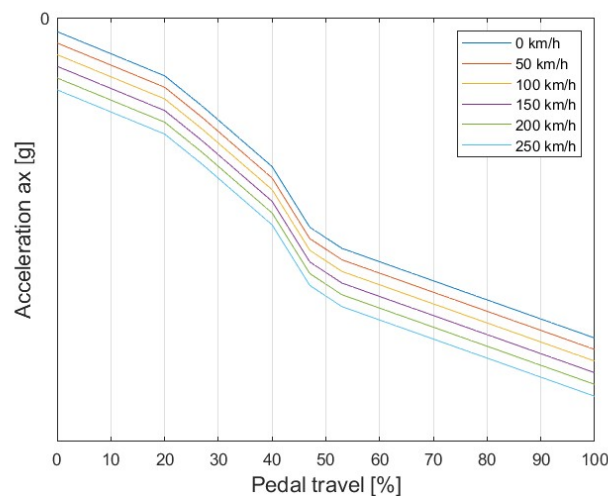


Figure 69: Deceleration profile as function of brake pedal travel and initial velocity

### 4.3. ELECTRIC MOTORS SIGNALS

Once clarified the longitudinal behaviour of the vehicle and the goal of the control unit to generate braking forces such to maintain constant deceleration, it is needed to analyse the behaviour of the two electric motors in P4 position during the braking manoeuvre.

From the road-testing signals in Figure 71, it is possible to see how e-motors collect a constant power converting kinetical energy back to electrical energy.

However, it is immediate to notice that the constant power region does not extend completely until the end of the braking manoeuvre (dotted line) but interrupts even if the driver is still braking and progressively reduces to zero.

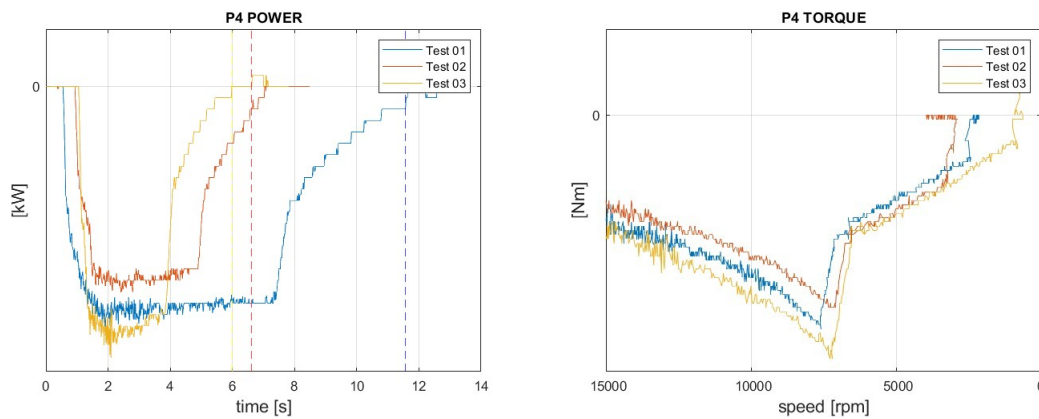


Figure 70: Electric motors torque signals (left)

Figure 71: Electric motors power signals (right)

The same trend can be seen on the collected signals referring to electric motor torque. As the vehicle decelerate, so the electric motors do, since their velocity is linked to wheels speed by a fixed transmission ratio.

As a consequence, the torque is expected to increase (in absolute value) proportionally to maintain a constant power according to  $T = \frac{P}{\omega}$ .

However, the real signal increase until a certain limit than saturates and start decreasing, even if the braking event is not concluded.

To understand this unexpected behaviour of regeneration, possible variables creating limits have been analysed.

- BATTERY LIMITS

The values of power recorded in the tests here reported, and all others analysed but not showed here for simplicity, appear to not be linked to the driver brake request, so a cause for this target constant value may be found on the battery side.

It must be considered that the three tests are performed in the same way but consecutively, so with a different initial state of charge of the battery.

From the technical papers of the battery itself, the following characteristic of maximum allowable power as function of the state of charge can be retrieved:

<i>State of Charge [%]</i>	<i>Maximum regenerative power [kW]</i>
25	140
50	115

*Table 9: Maximum battery regenerative power (10s @ 25°C) [3]*

The battery can work in a state of charge range between 25% and 95%.

Reconstructing the trend of maximum allowable regenerative power from the battery as function of the state of charge and analysing the level of charge in each test, it was possible to notice that the electric motors work with the goal to keep the constant power region at a value of 70% of the maximum admissible by battery.

Anyway, the real values are not reported in this thesis work for confidentiality reasons.

With these results, it is evident that the regenerative power never overcomes the admissible limit in the specific working conditions and does not even last for enough long to become cause of regenerative event to stop.

A further check on battery parameters can be found controlling to cell voltage value during regeneration and comparing it to the maximum value allowable, corresponding to 4.2V continuous from technical data sheets.

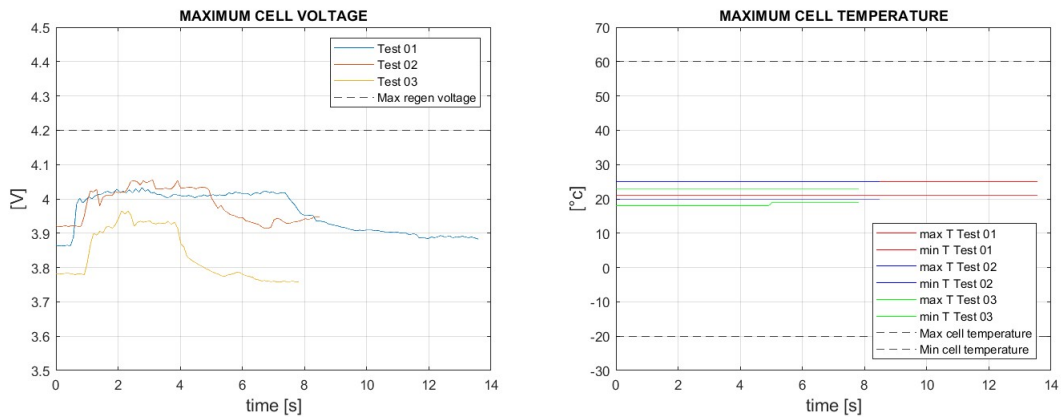


Figure 72: Maximum cell voltage (left)  
Figure 73: Maximum and minimum cell temperature (right)

In Figure 72 it is noticeable as the maximum cell voltage values collected by vehicle network signal never exceed the maximum one.

Also, the recorded signals referring to the cell maximum and minimum temperature in Figure 73 show how the operating range of  $-20^{\circ}\text{C}$ ;  $+60^{\circ}\text{C}$  is satisfied, confirming that the battery has not a limiting role in the regenerative event.

- ELECTRIC MOTORS LIMITS

Signals referring to electric motors' temperature were collected, showing that for this kind of manoeuvres the temperature increase is really limited, not forcing any temperature limitation strategy. In Figure 74 the trend of motor temperature for the three tests is reported.

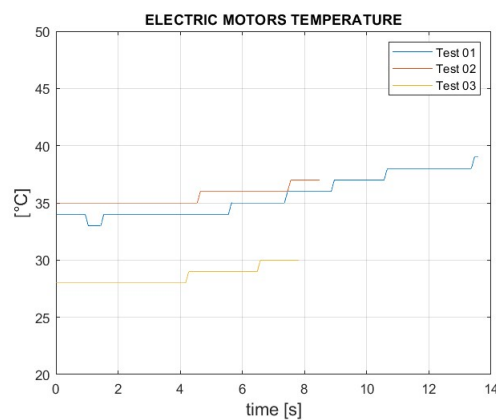


Figure 74: Motor temperature

Due to unavailability of technical information about electric motor characteristics, it is not possible to say with certainty that the temperature does not create any limit but being the deviation between start and end of the manoeuvre so low, it is reasonable to assume it, as said above.

Thanks to signals recorded during road testing and referring to the maximum torque generated by the motors, it is possible to reconstruct the motor characteristic. It can be noticed as all the lines referring to different tests overlap, leading to confirm that the diagram really represents the trend of maximum generable torque.

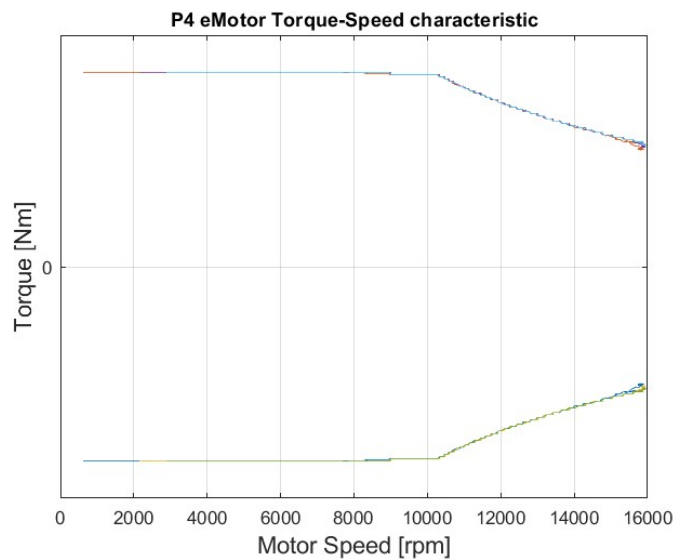


Figure 75: Electric motor torque-speed characteristic

Values of maximum torque are not reported for confidentiality reasons, but it can be seen that base speed corresponds to almost 10000 rpm.

On the other hand, in Figure 71 it is possible to notice how the constant power region, and so the increasing trend of torque, always stops when the electric motors are at the same rotational speed, of about 7500 rpm, different from base speed.

For this reason and since the maximum absolute value of torque recorded during the tests is different from the maximum one in Figure 75: Electric motor torque-speed characteristic, it can be assumed that the electric motors are not limiting regeneration.

- INVERTER LIMITS

Imputing the cause of end of regeneration before the end of manoeuvre to battery or to electric motors is not possible as seen above, so investigating the behaviour of the inverter is necessary. As seen in Chapter 3.3.3, when performing regenerative braking, this latter component has the role of managing the commutation of current such to create resistive torque and restoring energy coming from the road. For this purpose, the duty cycle of the six-switches bridge opening and closure must be such to guarantee the back electromotive force to be boosted up to battery charging voltage exploiting the properties of motor phase inductances.

Being the back emf proportional to motor rotational speed while battery charging voltage constant, the inverter duty cycle must change continuously, increasing as the vehicle slows down.

However, below a certain motor speed, the duty cycle increases in a steep way and the switches must be ON in the storing phase for such a long time to allow enough boosting of the back emf that the residual time for the energizing phase is not enough to transfer the collected energy to battery.

This speed threshold determines the end of regeneration and can be assumed to be the reason for which the trend of torque in Figure 71 has the described shape. In particular, the motor speed threshold for end of regeneration in this thesis analysis can be defined as 7500 rpm.

## 5. VEHICLE MODEL

Thanks to the data collected during road testing and analysing the signal of many different manoeuvres, it was possible to reconstruct the logics behind the energy recuperation during braking event for the vehicle studied in this thesis work, pointing out which are the main target parameters to be satisfied, the external inputs and the limits.

Many assumptions have been done to overcome data that were not possible to find and, to verify their correctness, the final part of this thesis work will be focused on developing a model of the braking system using *Simulink* environment to simulate the vehicle behaviour during braking event. The model will then be validated thanks to *VI Car Real Time* software that allows it to cooperate with an external vehicle model replicating the manoeuvres performed on track and checking the coherence of the results.

### 5.1. MODEL DEVELOPMENT

As said, the simulating model allows to investigate the vehicle behaviour under every possible condition and is particularly useful to replicate real situations recorded on test track and compare the outcome.

The model developed in this thesis work has been built with the use of *Simulink* software, in which it is possible to configure equations using graphical block to substitute traditional programming code, helping both the model construction and the control.

A traditional code written with *Matlab* software anyway joins the graphical tool in order to handle a faster control of the system by assigning desired values to important tuneable parameters and exporting results.

In particular, the layout of a braking control unit has been developed and tested and is now illustrated.

In Chapter 4, the logics behind regeneration have been investigated and can now be transposed into a programming code. First of all, external inputs that the braking control unit should receive and target values it has to satisfy must be defined.

The external inputs are mainly:

- Vehicle speed
- Wheels rotational speed
- Driver braking demand
- HV battery state of charge

Many other parameters can be continuously monitored by the braking control unit installed on a vehicle, such as tire pressure, estimation of coefficient of adherence of the road and brake temperature. This latter one in particular, is an important parameter affecting the braking efficiency and the whole longitudinal behaviour of the vehicle during braking events.

Without the possibility of monitoring this factor, due to absence of signal on the vehicle network, the assumption to always have brakes temperature constant and in the optimal working range has been done.

It must be considered that the manoeuvres considered concerns braking in straight and with constant pedal pressure: this is not the worst case for braking and do not stress the components as normal driving could do. For this reason, the assumption can be considered as coherent.

As a results of the braking control unit work, the outputs to be sent to electric motors and disk brakes are:

- Total braking torque required
- Maximum energy admissible by the battery
- Actual power regenerable by the electric motors
- Braking torque split between electrical and mechanical
- Variation of battery state of charge

The evaluation of these parameters is performed by the software of the braking control unit and has been replicated in the model in analysis.

For each of the outputs reported above, an overview of the way in which are estimated is provided in what follows, together with the description of the blocks composing the model.

### 5.1.1. TOTAL BRAKING TORQUE REQUIRED

The main goal of the braking control unit is to properly evaluate the amount of braking torque the vehicle requires to be stopped or decelerated as function of the driver request. In order to determine the braking torque, the first step is to settle the target deceleration profile to be followed by the vehicle, according to initial conditions. In the simulation model, this process is replicated by means of a look-up table, having the initial velocity and the brake pedal travel as input and the target constant deceleration as output. The table is composed of the values retrieved from the vehicle road tests as described in Chapter 4.2.

In Figure 77 a scheme of how the look-up table has been configured in the model is reported.

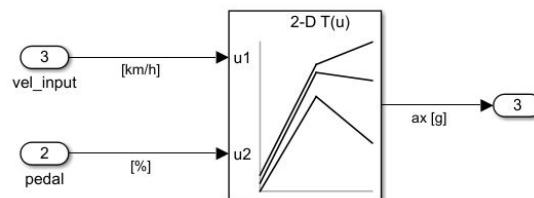


Figure 76: Deceleration look up table

The global layout of the deceleration profile evaluation is reported in Figure 77, with a further check on the driver request in terms of accelerator pedal stroke:

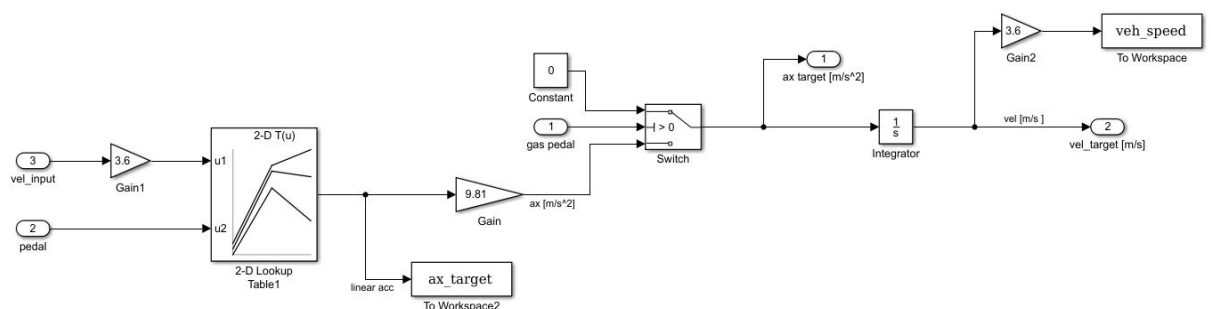


Figure 77: Target deceleration profile and velocity estimation

Whenever the gas pedal is released and the brake pedal is pressed, the braking control unit sets the deceleration resulting from the look-up table as the target. Without the check on the gas pedal position, the system could enter in a situation in which the control unit imposes coastdown deceleration as target one even if the driver is asking for traction: if the acceleration pedal is pressed, acceleration must be determined by tractive system and not by brake control unit.

The output of this simulation block in the end is the instantaneous deceleration and velocity the vehicle should follow, useful to determine the total instantaneous braking torque required.

For this purpose, the equations of longitudinal dynamics described in Chapter 1.4 have been implemented in the simulation environment. In particular, vertical force distribution can be calculated by the rotational equilibrium equation of the whole vehicle, considering the road inclination  $\theta$  and the geometric characteristic of the car as wheelbase  $L$ , distance of centre of gravity from rear axle  $b$ , centre of gravity height  $Hg$ , frontal area  $Af$  and mass  $m$ .

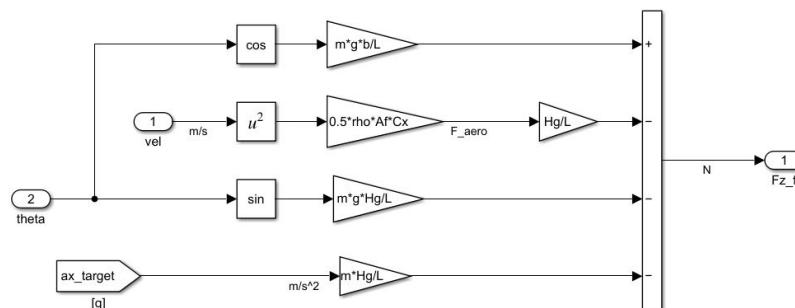


Figure 78: Vertical force distribution

From the target velocity and deceleration to be followed by the vehicle, it is possible to evaluate the longitudinal force on the tires needed to slow down the vehicle itself, from the longitudinal force balance. The rolling resistance has been estimated to be 2% of the total vertical force, while the aerodynamic force evaluated as function of the square of vehicle speed. The total longitudinal force developed between tires and ground will produce a braking torque which depends on the loaded wheel radius, here estimated as

97% of the unloaded one. A further contribution to the braking torque is provided by the wheel rotational inertia.

Figure 79 shows how this system has been modelled.

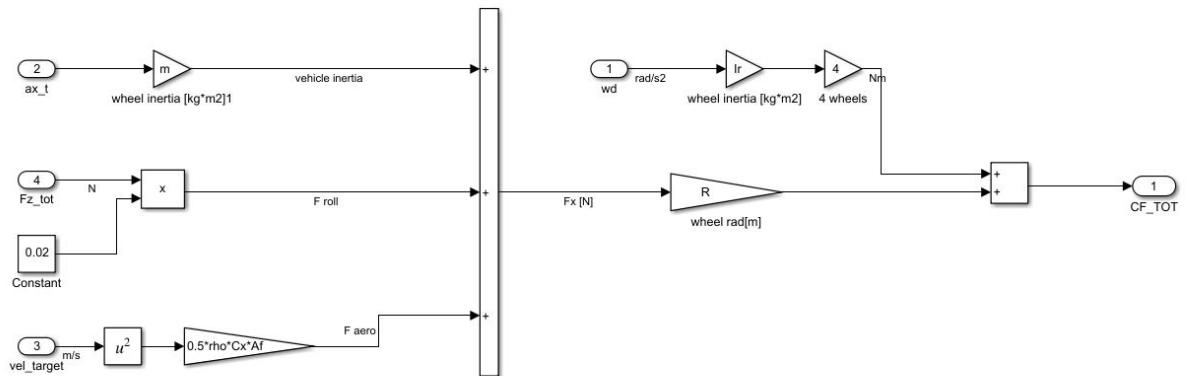


Figure 79: braking torque evaluation model

### 5.1.2. MAXIMUM CHARGING POWER ADMISSIBLE BY THE BATTERY

When dealing with energy recuperation important attention must be given to battery characteristics. For reliability and safety reasons, in fact, the Battery Management System BMS can impose limits regarding

- Current
- Voltage
- Temperature

during battery operations, to avoid a fast degradation of the State of Health of the battery itself. Many of these limitations have been discussed in chapter 4.3, focusing on how the most important design parameter to be considered during energy regeneration event is the power flowing into battery at each moment.

In particular, the maximum power admissible by the battery is function of the state of charge and is further reduced by an experimentally evaluated factor of 70%.

This limit has been modelled in simulation environment as reported in Figure 80:

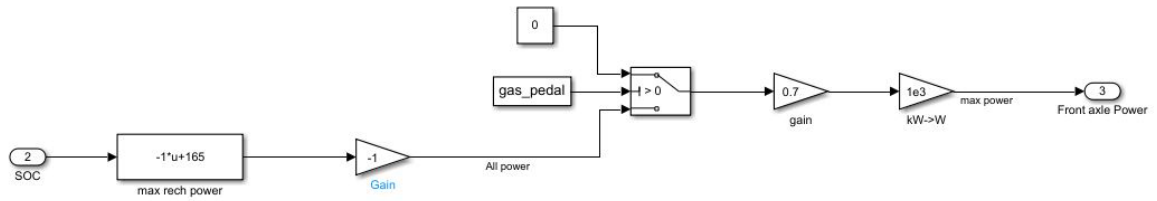


Figure 80: Maximum battery charging power

The switch reported in the scheme above is useful to discriminate if the driver is asking for power from the battery or not. In this case, if the accelerator pedal is pressed, the battery imposes no limits since regeneration is not occurring. As a future development of this thesis, the model could be completed with the maximum discharging power limits.

### 5.1.3. ACTUAL POWER REGENERABLE BY ELECTRIC MOTORS

Once the maximum charging power allowed by the battery has been defined, it is needed to quantify the actual power developed during regeneration by the front P4 electric motors. As described in chapter 4.3, analysing the signals collected during road testing, it was evident that the electric motors power behaviour was following a constant trend equal to 70% of maximum battery charge power for a while, then a ramp down until end of regeneration. The threshold between the two zones is defined by the speed limit imposed by the inverter, equal to a base speed of 7500 rpm. The ramp down when regeneration ends is then divided into two zones with different slope.

According to this statement, the motor has been modelled dividing the operating range in three main areas, as reported in the table below:

CONSTANT POWER REGION	RAMP DOWN 1	RAMP DOWN 2
$\omega_m \geq 7500\text{rpm}$	$7500 > \omega_m \geq 6500\text{rpm}$	$\omega_m < 6500\text{rpm}$
$T_1 = \frac{P}{\omega}$	$T_2 = m_1 \cdot \omega_m + k_1$	$T_3 = m_2 \cdot \omega_m + k_2$

Table 10: Electric braking torque regions

The model development has involved the electric motor torque, in order to control a parameter that more easily could be linked to the current flowing.

The two ramp-down areas differ for having a different slope, as can be noticed in the figure below.

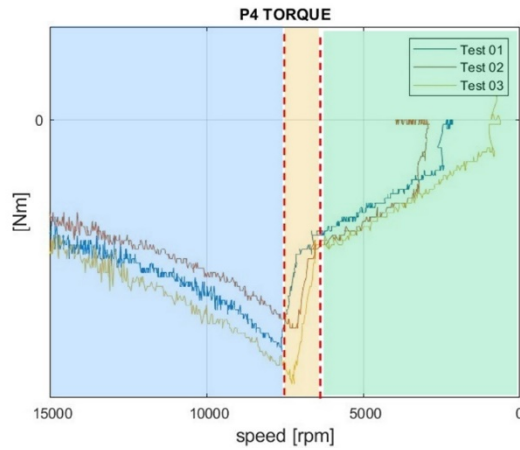


Figure 81: Electric motor torque

Three different subsystems have been developed for the three torque zones, each operating independently in its speed range. As output, the torque generated by the electric motor is evaluated, and so the actual power restored that can be transferred to the battery, considering losses due to component efficiencies.

Each block is illustrated in detail in the following.

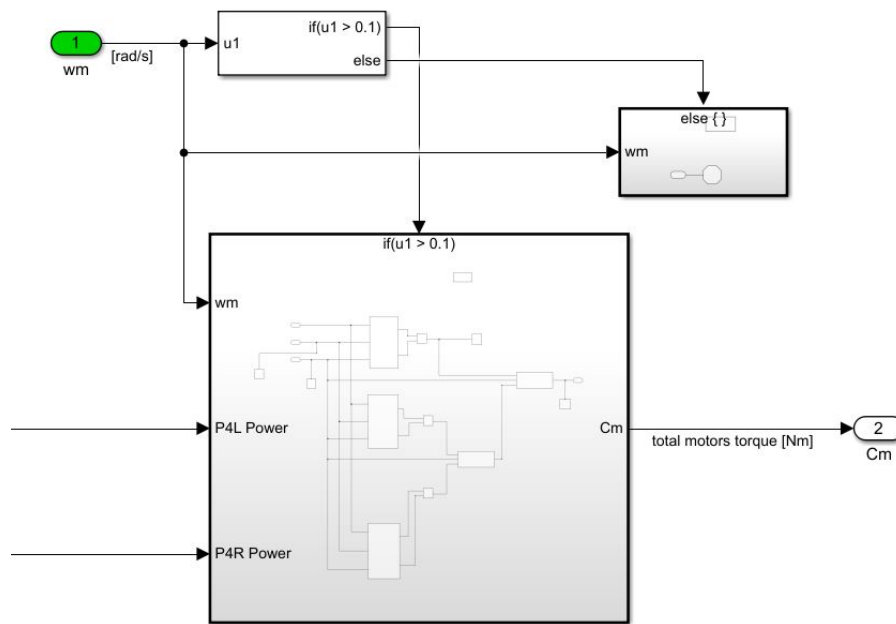


Figure 82: Motor model

First of all, the electric motors block needs to receive as input the maximum charging power for the battery, reduced by 30% for safety margin. The power will be divided equally between the left and the right electric motor since the model replicates the behaviour in straight direction.

As improvement, the model could be implemented with a control logic for braking in turn by receiving the speed signal independently from each wheel.

The motor speed input has been evaluated by considering a constant transmission ratio of 13.2 between the wheels and the electric motors.

An external control on the motor's speed is implemented in order to stop the simulation whenever this latter approaches zero speed.

In Figure 83, the configuration of electric motor torque evaluation is reported. It can be noticed that the choice of which subsystem consider as function of the instantaneous motors speed has been implemented with two switches.

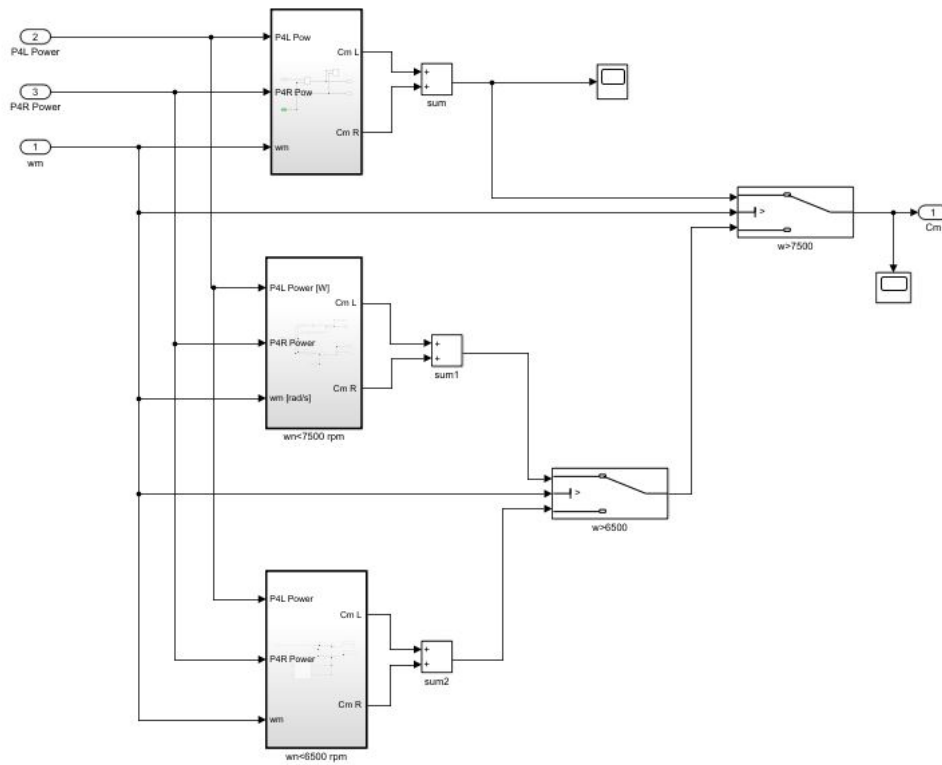


Figure 83: Motor torque split as function of speed

The first subsystem includes the equation to evaluate motor torque under the hypothesis of constant power and is selected as long as the motor speed is higher than 7500 rpm, so whenever energy recuperation is allowed by the inverter unit. The subsystem is composed as follows:

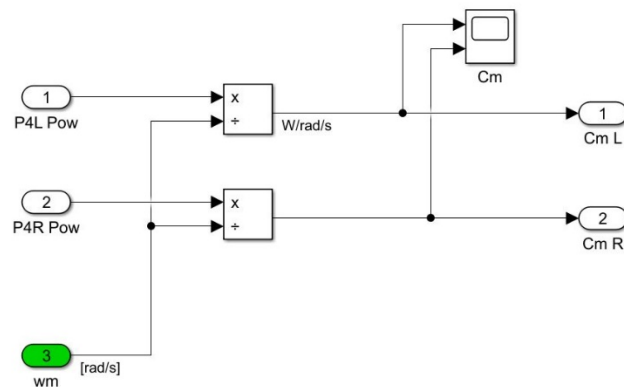


Figure 84: motor torque in constant power region

The other two subsystems are designed such to reproduce the torque trend lines of known slope and are selected when the motors speed become low. In these situations, the inverter module is no longer able to sustain energy recuperation and all the residual current flowing in the circuit is dissipated over the circuit internal resistances.

As final part of the electric motor analysis, the actual power is evaluated, useful to determine the amount of energy transferred to battery.

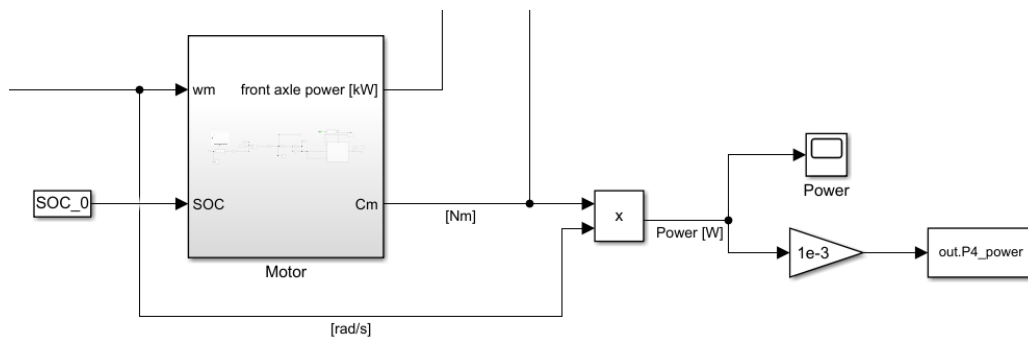


Figure 85: Actual electric motor power

#### 5.1.4. BRAKING TORQUE SPLIT BETWEEN ELECTRICAL AND MECHANICAL

Once evaluated the resistive torque generated by the electric motors it is possible to evaluate the remaining torque to be developed by the hydraulic braking system to have in the end the total required braking torque evaluated in 5.1.1.

Moreover, it is possible to figure out the percentage of electric braking torque produced.

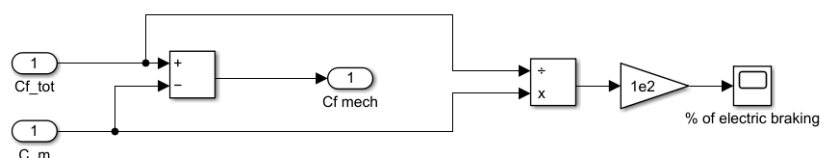


Figure 86: Braking torque split between electrical and mechanical

### 5.1.5. VARIATION OF BATTERY STATE OF CHARGE

During braking event, the resistive torque induced in the electric motor have the double effect to decelerate the vehicle and store energy to transfer to the battery.

Taking in consideration the efficiencies of both the electric motors and of the inverter unit, it is possible to determine the amount of instantaneous charging power flowing to battery.

This process is performed in the subsystem reported in Figure 87 and more in detail in Figure 88.

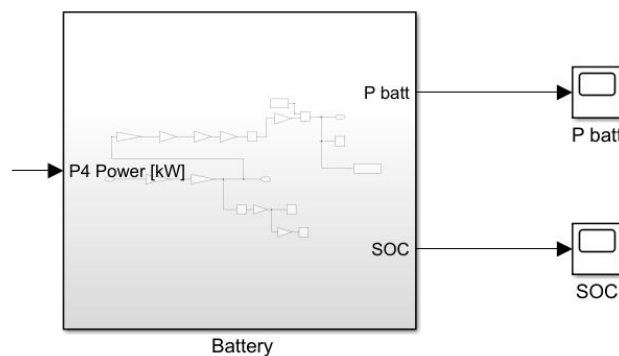


Figure 87: Battery model subsystem

The battery block includes specifications on the battery characteristics, as charging voltage, capacity, and initial state of charge.

From these specific, it is possible to retrieve the instantaneous current flowing into the battery pack and, integrating over time the ratio between current and capacity, the variation in state of charge.

$$\Delta(SOC) = \int_{t_0}^{t_1} \frac{I}{C} dt$$

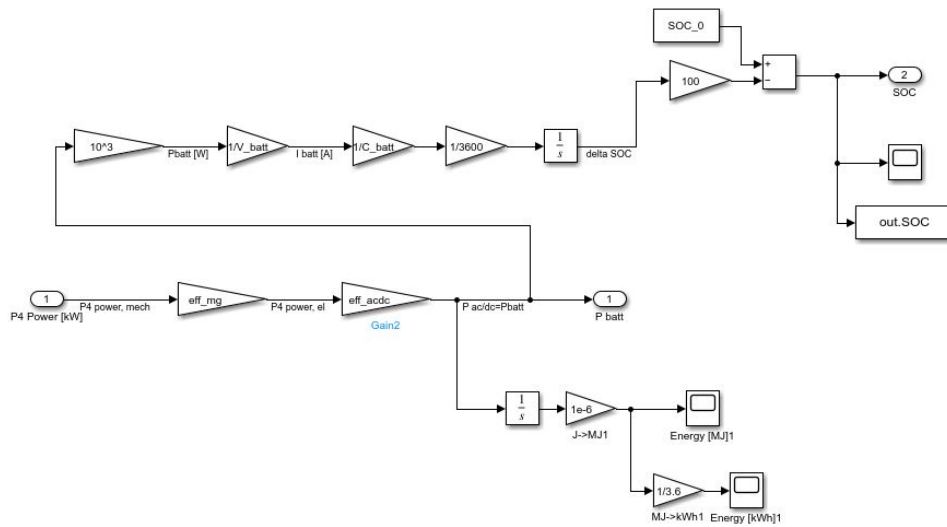


Figure 88: Battery model detail

## 5.2. MODEL VALIDATION

The model developed with the use of *Simulink* tools aims to replicate the longitudinal behaviour of the vehicle when subjected to braking intervention and estimate the energy flow toward battery.

To test the correctness of its work, it is needed to set up an environment in which the developed braking system model dialogs with an existing full vehicle model in a closed loop.

This has been done with *VI-Car Real Time* software from *VI grade*, a tool which can be interfaced with the *Matlab* environment.

The final goal is to check if the parameters evaluated by the braking system as described in 5.1 are such to satisfy the vehicle demand and to replicate the real behaviour of the vehicle as recorded during track tests. A great advantage of this simulation work is to properly consider many vehicle parameters that were not taken into account during the modelling, such as

- Tire behaviour: the full vehicle model includes Pacejka formula to evaluate the forces exchanged between tires and road.

- Vertical load distribution: from the vehicle model it is possible to consider the instantaneous distribution of vertical load with the effect of load transfer, while in the stand-alone braking model the static one was considered.
- Rolling radius: from the vehicle model it is possible to consider a more exact value of the instantaneous wheel radius, that was previously approximated as 97% of the unloaded one.
- Longitudinal slip: the vehicle model allows to have a good estimation of the slip value, defined in 1.1 as the deviation of the tire rotational speed from the rotational speed that a rigid body with the same radius would have.

Considering these parameters and many others provided by the vehicle model, it is possible to build a more sophisticated system really reproducing the vehicle behaviour and check if the total braking torque evaluated is sufficient to stop it with the desired deceleration.

In this chapter, an overview of how the co-simulation has been designed is described and the analysis of the results obtained is provided.

The model has been tested over straight braking manoeuvres with constant brake pedal stroke, in order to check the correspondence to the data recorded during track tests session.

### 5.2.1. CO-SIMULATION DESIGN

To let the full vehicle model and the developed braking control unit subsystem interact, a *VI-CarRealTime* mask has been introduced and the input and output parameters of the mask have been selected between all those available.

In particular, input parameters to be given to the vehicle model are:

- Braking torque on each tire
- Constant zero value to deactivate internal braking system

Output parameters retrieved from the model and transferred to the braking control unit or used for results analysis are:

- Longitudinal forces on the tires
- Normal forces on the tires
- Wheels rolling radius
- Longitudinal Slip
- Longitudinal vehicle velocity
- Longitudinal vehicle acceleration

The complete model interface layout is reported in Figure 89.

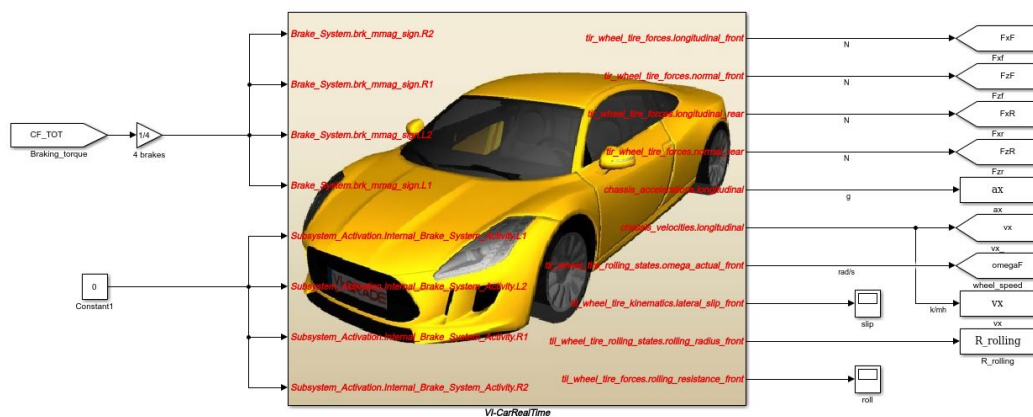


Figure 89: Input/output parameters of VI-CarRealTime mask

The parameters retrieved as output from the VI-CarRealTime mask are transferred to the braking model subsystems. For example, the vertical forces are not anymore evaluated as in Figure 78 from the static equilibrium equations but recalled from vehicle model. The same process is adopted for the rolling radius. The longitudinal forces are evaluated as illustrated above in Figure 79 and compared to those retrieved for the model.

This allows to have more accurate values that consider not only the static vehicle approximation but also the internal vehicle characteristics and to close the loop between braking system and vehicle model.

The updated vehicle model is reported in the figure below.



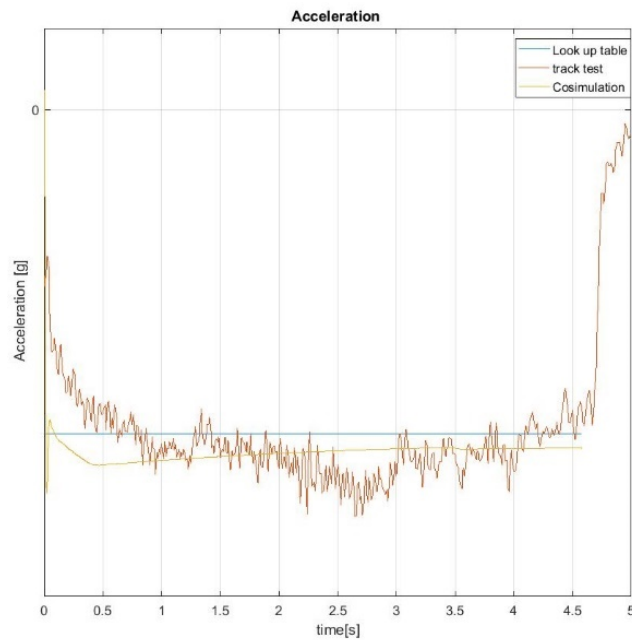


Figure 91: Acceleration comparison: Target, Actual, from vehicle model

From the deceleration trend reported in Figure 91 it is possible to analyse the difference the results from simulation, in orange, have from the road test recorded ones in red.

The line in blue, instead, represents the target deceleration imposed by the braking model by means of a Look up table, determined as function of brake demand and initial velocity. It is possible to point out as it appears to be underestimated with respect to the real deceleration trend. This can be motivated by the low amount of data to rely on during the look up table estimation.

The deviation between the target value of deceleration in blue and the one resulting from *VI-Car Real Time* cosimulation in orange is limited but anyway present. In the first part of the manoeuvre, as the driver start pressing the brake pedal, a transient phase is present in which the vehicle starts decelerating, reaching a constant value after a short time.

Net of some noise naturally present in the acquired signal, due to analog to digital conversion and to the absence of filtering, the simulated behaviour of the vehicle results in being coherent with the real one, assuming its average value.

It is necessary to point out how the acquired signal results from a real track test, in which the manoeuvre is performed by a human driver and the pression on the brake pedal is not exactly constant as should be. The brake pedal stroke trend, instead of being flat, oscillates

around the target value, with a deviation of around  $\pm 3\%$ . The driver request for this manoeuvre has been reported in Figure 64 (test3).

It can be concluded that the total braking torque evaluated in the model of Figure 79 ends up in decelerating the vehicle more than required. This can be motivated by the presence of an overestimated vehicle inertia or underestimated rolling resistance force: both parameters are involved and contribute during the manoeuvre in the braking response.

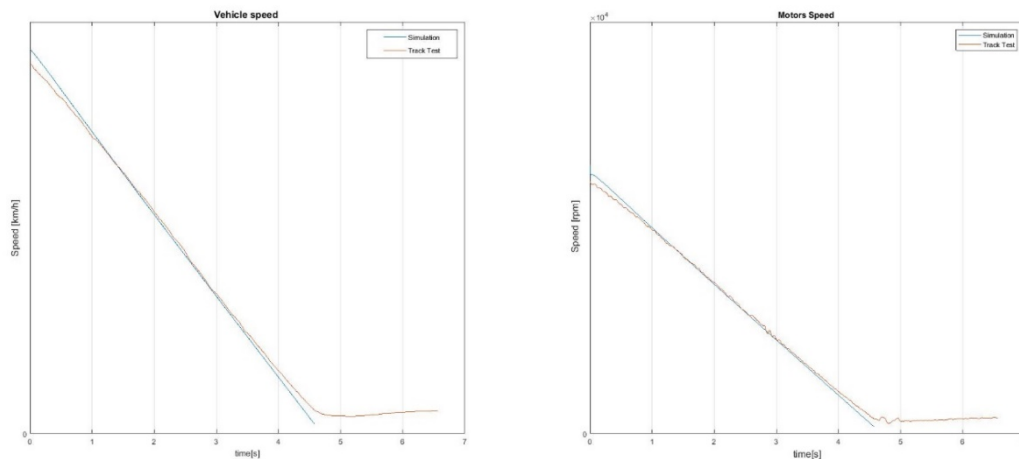


Figure 92: vehicle velocity comparison: from vehicle model, actual (left)  
Figure 93: e-motor velocity comparison: from vehicle model, actual (right)

In the figures above the velocity trend of the whole vehicle and of the electric motors are reported. They differ each other of a quantity representative of the transmission ratio  $\tau$  and of the wheel rolling radius.

It can be noticed again how the simulated deceleration results to be higher than the real one, for the same reasons explained before.

Globally, the simulated vehicle behaviour can anyway be considered reliable.

For what concerns the electric motors' behaviour, the regenerated energy and the electric braking torque produced are now reported and described.

In Figure 94 the electric torque is compared: the signals collected from the vehicle network, in orange, refer to the actual torque recorded on the P4 e-motors, depending on the manoeuvre conditions. The plot in blue, instead, refers to the simulated vehicle behaviour, reproduced with the Simulink model of Figure 83.

When referring to energy recuperation during braking, the electric motors behave differently depending on their rotational speed, and the generation of electric braking torque follows different logics. To sum up, it is possible to observe how the braking torque increases in absolute value as the braking manoeuvre begins, to be then reduced as soon as the inverter limit speed is reached. The maximum torque generatable by the electric motors if no external limits were occurring has been reported in Figure 75.

A deeper explanation of the reasons for which the electric braking torque is limited has been provided in chapter 4.3.

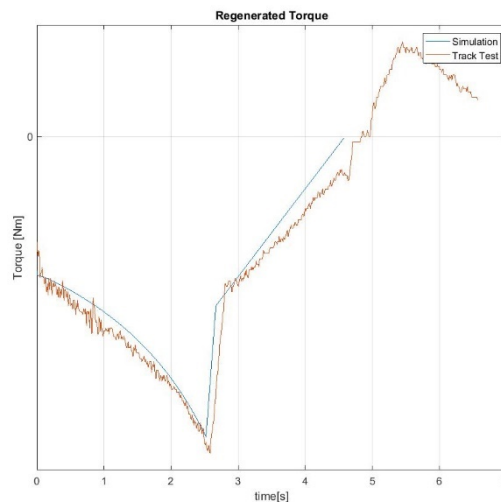


Figure 94: Electric motor braking torque comparison

By knowing the amount of electric braking torque instantaneously produced and the rotational speed of the electric motors, it was possible to evaluate the amount of regenerated power, according to the equation

$$P = T \cdot \omega$$

In Figure 95 the recorded regenerated power is compared to the simulated one. It is possible to observe how the two trends almost overlap, with a small deviation only in the initial part, due to the transient oscillation of torque.

In conclusion, it is possible to assume that the results of co-simulation well reproduce the real electric motors' behaviour.

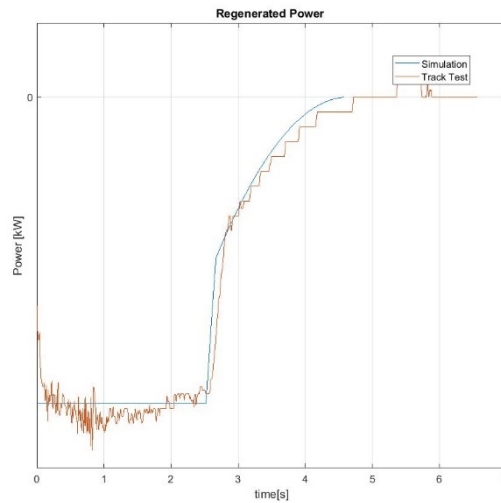


Figure 95: Electric motor power comparison

Once evaluated the total amount of braking torque needed to decelerate the vehicle with a target deceleration profile and the amount of braking torque delivered by the electric motors, it is possible to perform an analysis that leads to understanding what percentage of residual torque should be actuated by the mechanical disk brakes.

It is known that regenerative braking should always be coupled with traditional mechanical brakes for safety reasons; moreover, this analysis shows how often the level of braking torque produced during regeneration is so low that the intervention of disk brakes is needed for the whole duration of the manoeuvre.

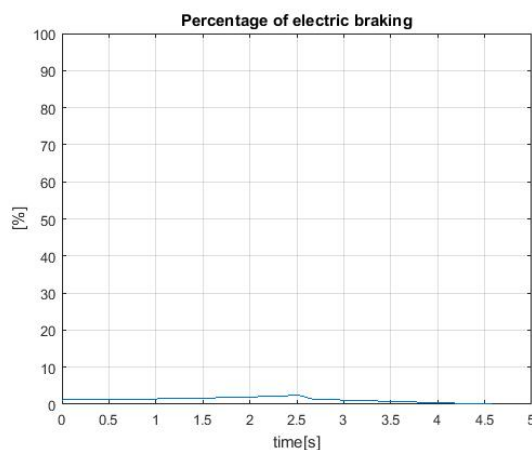


Figure 96: Percentage of electric braking during brake-step manoeuvre

In Figure 96 the amount of electric braking torque over the total one needed is reported. It can be noticed how low it is, never sufficient to stop the vehicle neither to decelerate it in the correct way.

This behaviour has been checked with an analysis on the battery nominal characteristics, that led to conclude that the battery itself is small compared to the dimensions that should have to allow complete energy recuperation.

The power flows that the component can receive are high, up to 100 kW depending on the instantaneous state of charge, but not sufficient to generate a braking torque high enough to avoid the mechanical braking intervention.

A further confirmation of the important role of the disk brakes has been found analysing the signals coming from vehicle network regarding the pressure on the brake pipes. By knowing the geometrical characteristics of the brakes actuators (surface  $S$ ) and the disk diameter  $D$ , estimating the efficiency  $\varepsilon$  and the friction coefficient of the brake pads  $f$ , it has been possible to evaluate the amount of braking torque  $T$  that the recorded pressure  $p$  on the line generates, according to the equation:

$$T = p \cdot S \cdot \varepsilon \cdot f \cdot \frac{D}{2}$$

In Figure 97, the estimated torque has been compared to the simulated one deputed by the electrical torque amount. The two trends are almost overlapping, leading to conclude that the simulated vehicle model behaves like the real one and that the amount of braking torque required at mechanical brakes level is as high as expected.

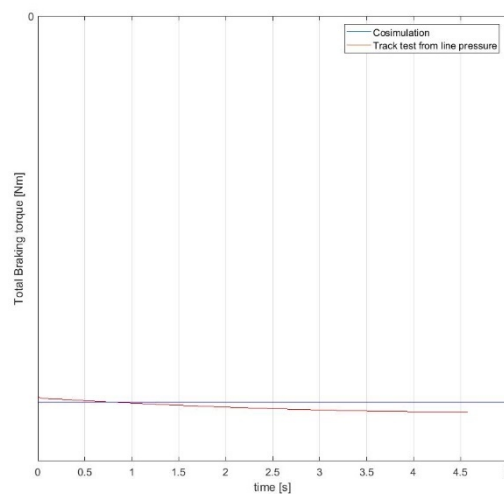


Figure 97: Braking torque comparison

In the end, the amount of regenerated power by the electric motors and transferred to the battery allows to perform an estimation on the variation of the state of charge, according to what described for the battery model of Figure 87.

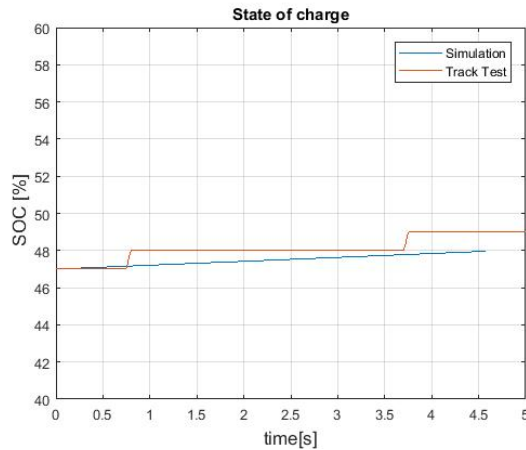


Figure 98: Battery state of charge comparison

By the trend reported above it is possible to observe that the simulated vehicle model faithfully reproduces the recorded behaviour.

An important consideration can be done by noticing how the increase in state of charge during the manoeuvre is up to +2%, large amount considering the short duration of the test. Anyway, it is important to recall that the battery with which the vehicle is equipped is small and that the incoming power flows are instead huge, even if not lasting for long. These considerations lead to understanding that for the analysed vehicle the regeneration strategy is performed with the primary goal of recharging the battery and increase the electrical driving range, and not with the target of braking the vehicle.

The analysis described above with a comparison of the main vehicle parameters between the recorded and the simulated ones has been repeated by changing the initial conditions of vehicle speed, battery state of charge and braking demand, and the results have been sufficiently satisfying to consider the vehicle model reliable, even with the assumptions performed and described in the chapters above.

## CONCLUSIONS AND FUTURE DEVELOPMENT

The time spent in collaboration with Danisi Engineering s.r.l. company and this report aim to the regenerative braking control logic evaluation through a reverse engineering process of a hybrid supercar.

This project can be considered a good starting point to investigate the way in which this active system works and its integration on the vehicle, with an analysis on the characteristics of the components involved in the process.

The evaluation of the regenerative braking system control logics has been limited to the study of vehicle behaviour during braking manoeuvres on a straight road, neglecting the vehicle performance during cornering events.

This choice has been adopted for the double reasons of limiting the amount of work to be coherent with what required by the university and to have more time available to deeply investigate the components' behaviour in one only manoeuvre.

Moreover, it is worth to point out that the track tests on which this thesis work rely on have not been performed specifically for this project's purpose but for company's reasons, so the manoeuvre's study had to count on a restricted number of tests.

A possible future improvement of the present thesis work could, indeed, be developed by bringing again the vehicle to a track and performing tests specifically aimed at understanding electric braking behaviour. Possible tests to be performed could be progressive braking and braking step manoeuvre in every possible powertrain setting, as hybrid, pure electric, sport or race ones.

Equipping the vehicle with a larger number of sensors, specifically designed for this study, could be a good improvement too, allowing to have important signals to be analysed, such as current and voltage value of each e-motor's phase, mainly to study the electric traction's components behaviour.

Globally, the data analysis gave satisfactory results, pointing out some unexpected actions taken by the vehicle components to limit the regenerative braking event.

It is necessary to recall that for this specific supercar, the adopted high voltage battery is small. The amount of energy recovered during the braking manoeuvre, indeed, turned out to be limited by the battery dimensions, and definitely not enough to brake the vehicle of the desired amount.

For this reason, a deep analysis on how the traditional hydraulic brakes intervene and cooperate with the electric braking has been performed too.

The study on the brake blending strategy adopted on this vehicle confirmed the initial hypothesis performed on having a constant target deceleration. This choice, indeed, finds large corroboration on a legislative basis <sup>[11]</sup>, since having constant deceleration contribute on having a better drivability feeling, larger occupants' comfort and safety.

The developed braking system model gave satisfactory results in replicating the vehicle behaviour in braking events and estimating the power flow to the battery unit and the variation in its state of charge.

The integration of this subsystem in a complete vehicle model previously developed by the company vehicle dynamics' department revealed the coherence of the work with the expected results, based on the collected data on track tests.

This work can be considered complete itself for the purpose of the Master' degree final exam and a good starting point for future developments as previously described.

## BIBLIOGRAPHY

- [1]. Race car vehicle dynamics- Milliken Milliken
- [2]. Meccanica dell'autoveicolo- Giancarlo Genta
- [3]. Danisi engineering sensors and components technical datasheets
- [4]. Electronic systems for vehicles, didactical lectures, Prof. Crovetto Paolo Stefano
- [5]. Electrical drives for eMobility, didactical lectures, Prof. Bojoi Iustin Radu
- [6]. E-powertrain components, didactical lectures, Prof. Ravello Vittorio
- [7]. Mathworks theory for BLDC motors, <https://explore.mathworks.com/brushless-dc-motors-introduction/chapter-1-53QT-6225P.html>
- [8]. Model Based Development of Mild Hybrid Electrical Battery Systems, Master of Science Thesis, Mohanapriya Anandaguru Andreas Eriksson
- [9]. [www.quattroruote.it](http://www.quattroruote.it)
- [10]. Electric Powertrain control: an adaptable simulink model of torque path and validation by model in the loop, Tesi di laurea magistrale, Domenico Barile
- [11]. Regulation No 13-H of the Economic Commission for Europe of the United Nations (UN/ECE) — Uniform provisions concerning the approval of passenger cars with regard to braking [2015/2364]
- [12]. [www.researchgate.net](http://www.researchgate.net)
- [13]. <https://www.toppr.com/ask/content/concept/3-phase-ac-generator-209846/>
- [14]. <https://www.pmdcorp.com/resources/type/articles/get/regenerative-braking-part-i-steady-state-analysis-article>
- [15]. Driving and Braking Control of PM Synchronous Motor Based on Low-resolution Hall Sensor for Battery Electric Vehicle, Chinese Journal of mechanical engineering, Gu Jing, Ouyang Minggao\*, Li Jianqiu, Lu Dongbin, Fang Chuan, and Ma Yan
- [16]. Investigation of Regenerative Braking Performance of Brushless Direct Current Machine Drive System, Omer Cihan Kivanc and Ozgur Ustun
- [17]. Digital Pulse-Width Modulation Control in Power Electronic Circuits: Theory and Applications, Angel V. Peterchev

## LIST OF FIGURES

Figure 1: Wheel reference frame .....	2
Figure 2: Contact pressure distribution during braking and traction.....	2
Figure 3: instant point of rotation in pure rolling C, braking C' and traction C'' .....	3
Figure 4: Longitudinal friction coefficient as function of slip .....	4
Figure 5: Longitudinal friction coefficient as function of slip and Fz .....	4
Figure 6: Distorsion of contact patch .....	5
Figure 7: Pressure and slip distribution of a cornering tyre .....	6
Figure 8: Lateral force, caster trail and self-aligning torque as function of slip angle.....	6
Figure 9: Cornering stiffness as function of vertical load.....	7
Figure 10: Gough diagram.....	7
Figure 11: Effect of camber angle on Side force and Self-aligning torque.....	8
Figure 12: Interaction between longitudinal and lateral slip.....	9
Figure 13: Polar diagram of force exerted on tyres. a) experimental b) elliptical approximation.....	10
Figure 14: Elliptical model approximation .....	10
Figure 15: Vehicle fixed and local reference frame.....	11
Figure 16: Bicycle model reference frame.....	11
Figure 17: Understeering behaviour .....	14
Figure 18: Understeering curvature radius behaviour.....	14
Figure 19: Steering angle during Ramp steer manoeuvre .....	15
Figure 20: Steering angle as function of lateral acceleration during Ramp Steer manoeuvre .....	16
Figure 21: Side slip angle as function of lateral acceleration during Ramp Steer manoeuvre.....	16
Figure 22: Steering angle, lateral acceleration, slip angle and yaw rate trend during step steer manoeuvre	18
Figure 23: system response delay- step steer manoeuvre .....	19
Figure 24: vehicle longitudinal dynamics reference system .....	20
Figure 25: Power needed for motion on a flat road .....	21
Figure 26: MEMS accelerometer structure [4] .....	24
Figure 27: accelerometer technical data [3].....	25
Figure 28: Inertial measurement unit technical data [3] .....	26
Figure 29: Optical sensor (laser) technical data [3] .....	27
Figure 30: Optical sensors technical data [3] .....	28
Figure 31: Load cell technical data [3] .....	29
Figure 32: Steering angle, torque and speed sensor technical data [3] .....	30
Figure 33: Linear position sensor [4].....	32
Figure 34: : Linear position sensor technical data [3].....	32
Figure 35: Global layout of vehicle sensors positioning [3].....	33

Figure 36: Optical sensors for vehicle height (left) and side slip angle (right).....	34
Figure 37: Steering torque sensor .....	34
Figure 38: Load cell on brake pedal .....	35
Figure 39: Potentiometer .....	35
Figure 40: IMU system positioning .....	35
Figure 41: Data acquisition system [3] .....	37
Figure 42: Hybrid classification [6].....	39
Figure 43: e-traction classification: P method [8].....	40
Figure 44: Vehicle powertrain layout [9].....	40
Figure 45:P1 architecture [5] .....	41
Figure 46: Pure electric traction layout [9] .....	42
Figure 47: Hybrid traction layout[9].....	43
Figure 48: Regenerative braking layout[9] .....	43
Figure 49: Split strategies of brake demand: series(left) and parallel(right) phasing [10].....	44
Figure 50: Coil in an external magnetic field with current flowing through and force applied .....	47
Figure 51: electric motor single phase equivalent circuit [14].....	48
Figure 52: Dependence of back electromotive force on motor speed.....	48
Figure 53: Trend of torque as function of current.....	49
Figure 54: Net voltage in the cycle as function of motor speed.....	49
Figure 55: Brushless motor-generator layout [13] .....	50
Figure 56:PM rotor in an external magnetic field (grey) .....	50
Figure 57: DC/AC converter with half bridge circuit architecture [12].....	51
Figure 58:6 steps commutation – Traction [15].....	52
Figure 59:6 steps commutation – Braking [15].....	53
Figure 60: Boost converter circuit [12].....	54
Figure 61: Storing phase of regenerative braking [16] .....	55
Figure 62: Energizing phase of regenerative braking [16].....	55
Figure 63: Drivel brake pedal history .....	57
Figure 64: Brake step tests- driver brake demand.....	58
Figure 65: Brake step tests- acceleration .....	59
Figure 66:: Brake step tests- vehicle speed.....	59
Figure 67: Deceleration pattern over tests(left) .....	60
Figure 68: Linear interpolation of deceleration profile(right).....	60
Figure 69: Deceleration profile as function of brake pedal travel and initial velocity .....	61
Figure 70:Electric motors torque signals(left) .....	62
Figure 71: Electric motors power signals (right) .....	62
Figure 72: Maximum cell voltage (left).....	64
Figure 73: Maximum and minimum cell temperature (right) .....	64
Figure 74: Motor temperature.....	64

---

Figure 75: Electric motor torque-speed characteristic .....	65
Figure 76: Deceleration look up table.....	69
Figure 77: Target deceleration profile and velocity estimation .....	69
Figure 78: Vertical force distribution.....	70
Figure 79: braking torque evaluation model .....	71
Figure 80: Maximum power admissible by battery .....	72
Figure 81: Electric motor torque.....	73
Figure 82: Motor model.....	74
Figure 83: Motor torque split as function of speed.....	75
Figure 84: motor torque in constant power region.....	75
Figure 85: Actual electric motor power .....	76
Figure 86:Braking torque split between electrical and mechanical .....	76
Figure 87: Battery model subsystem.....	77
Figure 88: Battery model detail .....	78
Figure 89: Input/output parameters of VI-CarRealTime mask .....	80
Figure 90: Vehicle model .....	81
Figure 91: Acceleration comparison: Target, Actual, from vehicle model.....	82
Figure 92: vehicle velocity comparison: from vehicle model, actual (left) .....	83
Figure 93: e-motor velocity comparison: from vehicle model, actual (right) .....	83
Figure 94: Electric motor braking torque comparison .....	84
Figure 95: Electric motor power comparison.....	85
Figure 96: Percentage of electric braking during brake-step manoeuvre.....	85
Figure 97: Braking torque comparison .....	86
Figure 98: Battery state of charge comparison .....	87

## ACKNOWLEDGEMENTS

This thesis is the final work of many years of studying and of an internship period that helped me growing both from educational and human point of view.

For this great opportunity I would like to thank Danisi Engineering s.r.l., in particular to Patrick Giofrè and Claudio Ricci, for the way they welcomed me, their daily update and support in developing this project.

A huge thank you to the colleagues of *Box 5* for their help, friendship and for the good time spent together.

I would like to offer my special thanks to my academic supervisor, Professor Paolo Stefano Crovetto for the constant willingness and the support in developing the thesis.

## RINGRAZIAMENTI

La tesi presentata si pone come elemento finale di un percorso di studi intenso e di un periodo di stage aziendale che mi ha permesso di crescere dal punto di vista formativo ed umano allo stesso tempo.

Per questa grande opportunità tengo a ringraziare la Danisi Engineering s.r.l. tutta, nelle persone di Patrick Gioffrè e Claudio Ricci per la disponibilità e l'affiancamento quotidiano fornitomi. Un sentito, immenso, grazie ai colleghi del *Box 5* per l'accoglienza, il sostegno ed i momenti trascorsi.

Ringrazio il mio relatore, Professor Paolo Stefano Crovetto per il supporto nello sviluppo di questo progetto, nella stesura della tesi e durante il corso.

Molti sono stati i momenti felici durante il mio percorso di studi ed altrettanti quelli in cui si è reso necessario conforto e supporto. Mamma, Papà, Paolo, grazie di esserci sempre stati, per festeggiare o per sostenermi con la parola giusta. Questo traguardo è frutto dell'impegno condiviso di tutti noi. Grazie ai Nonni per il continuo sostegno.

Non sarà facile riassumere in poche righe l'importanza che l'amicizia ha avuto per me in questi anni, ci provo:

Grazie a Luisa, più sorella che amica, per i ricordi d'infanzia, per tutti i brindisi agli esami superati di entrambe, per le risate, i momenti condivisi, i viaggi e per avermi saputo dire sempre le parole giuste anche quando non le volevo sentire. È bello esserci stata alla tua laurea ed ora vederci crescere entrambe.

Martina, Giulia, Elisa, da un po' di anni a questa parte vi sorbite i miei periodici up&down e avete sempre i consigli giusti da darmi, prometto di ascoltarli un po' di più! Grazie per avermi permesso di condividere con voi i traguardi importanti di tutte e di essermi state accanto in questo. Grazie per i viaggi, per i km che avete fatto per seguirmi in gara, per gli spritz sui balconi delle vostre nuove case e per tutto quello di bello che ancora deve venire.

---

Grazie ai compagni incontrati in questi anni di studi che hanno reso il percorso più leggero, Eleonora prima tra tutti, sempre presente dai banchi delle scuole superiori e Penelope, incontrata nelle aule del Politecnico tra uno scambio di appunti e l'altro. Ci vediamo poco ma voglio molto bene ad entrambe.

Grazie a Jacopo, amico, compagno di studi e di concerti.

Dei molti colleghi con cui ho condiviso le fatiche (a volte molte!) della laurea magistrale ringrazio particolarmente Andrea e Marco, dapprima compagni e poi amici, studiare con voi ha reso tutto molto più leggero.

Grazie a Stefano, Marta e Federico, per i momenti universitari ma soprattutto per quelli condivisi in montagna, a camminare nel nostro mondo.

Infine, ringrazio il gruppo inseparabile di amici conosciuti durante il percorso di laurea triennale, diventato ormai famiglia, Giuseppe, Giorgia, Luigi, Matteo, Francesco, Antonio, Fabrizio, Mattia, Pierpaolo, Alessandro. Gli esami preparati in aula studio, le partite a calcetto durante le pause, i viaggi in Sicilia, le grigliate in campagna e le pizzate in 15 organizzate in un monocale sono state quanto di più bello mi ricorderò di questi anni.

Vi voglio bene.

